ANTIOXIDANTS & REDOX SIGNALING
Volume 26, Number 2, 2017

DOI: 10.1089/ars.2016.6677

ORIGINAL RESEARCH COMMUNICATION

Selective Disruption of Respiratory Supercomplexes as a New Strategy to Suppress Her2^{high} Breast Cancer

Katerina Rohlenova,[1,*] Karishma Sachaphibulkij,[2,*] Jan Stursa,[2–4] Ayenachew Bezawork-Geleta,[2] Jan Blecha[1], Berwini Endaya,[2] Lukas Werner,[4] Jiri Cerny,[1] Renata Zobalova,[1,2] Jacob Goodwin,[2] Tomas Spacek,[5] Elham Alizadeh Pesdar,[2] Bing Yan,[2] Maria Nga Nguyen,[2] Magdalena Vondrusova,[1] Margaryta Sobol,[6] Petr Jezek,[5] Pavel Hozak,[6] Jaroslav Truksa,[1] Jakub Rohlena,[1] Lan-Feng Dong,[2] and Jiri Neuzil[1,2]

Abstract

Aims: Expression of the *HER2* oncogene in breast cancer is associated with resistance to treatment, and Her2 may regulate bioenergetics. Therefore, we investigated whether disruption of the electron transport chain (ETC) is a viable strategy to eliminate Her2^{high} disease.
Results: We demonstrate that Her2^{high} cells and tumors have increased assembly of respiratory supercomplexes (SCs) and increased complex I-driven respiration *in vitro* and *in vivo*. They are also highly sensitive to MitoTam, a novel mitochondrial-targeted derivative of tamoxifen. Unlike tamoxifen, MitoTam efficiently suppresses experimental Her2^{high} tumors without systemic toxicity. Mechanistically, MitoTam inhibits complex I-driven respiration and disrupts respiratory SCs in Her2^{high} background *in vitro* and *in vivo*, leading to elevated reactive oxygen species production and cell death. Intriguingly, higher sensitivity of Her2^{high} cells to MitoTam is dependent on the mitochondrial fraction of Her2.
Innovation: Oncogenes such as *HER2* can restructure ETC, creating a previously unrecognized therapeutic vulnerability exploitable by SC-disrupting agents such as MitoTam.
Conclusion: We propose that the ETC is a suitable therapeutic target in Her2^{high} disease. *Antioxid. Redox Signal*. 26, 84–103.

Keywords: mitochondrially targeted tamoxifen, HER2, respirasome, breast cancer, mitochondria

Introduction

Functional electron transport chain (ETC) is essential for tumorigenesis (51, 57). At the same time, ETC is important in normal cells by providing a milieu permitting biosynthesis of aspartate and pyrimidine nucleotides, and for ATP generation (3, 47, 50). Classical pharmacological ETC inhibitors such as rotenone, antimycin A, or potassium cyanate have systemic toxicity, while available nontoxic ETC inhibitors such as the antidiabetic drug metformin are not potent enough and show little benefit for cancer patients in a number of clinical trials (18, 23, 35). Therefore, effective agents that would selectively target ETC in specific subsets of cancer cells are sorely needed.

ETC resides in the cristae region of the inner mitochondrial membrane (IMM). It comprises four respiratory complexes (termed CI-CIV) that further assemble into higher molecular structures called supercomplexes (SCs), increasing ETC efficiency and regulating substrate utilization (1, 21). ETC generates electrochemical gradient across the IMM referred to as the IMM potential ($\Delta\Psi_{m,i}$). This is essential for ATP production by mitochondrial ATP synthase and also allows cargo delivery into mitochondria using cations such as the triphenylphosphonium (TPP^+) group (28), which can therefore be used to bring ETC inhibitors close to their molecular targets (9). The level of ETC organization in various subsets of cancer cells, while largely unexplored, could be associated with differences in sensitivity to ETC inhibition.

[1]Institute of Biotechnology, Czech Academy of Sciences, BIOCEV, Vestec, Prague-West, Czech Republic.
[2]School of Medical Science, Griffith University, Southport, Australia.
[3]Prague Institute of Chemical Technology, Prague, Czech Republic.
[4]Biomedical Research Center, University Hospital, Hradec Kralove, Czech Republic.
[5]Institute of Physiology, Prague, Czech Republic.
[6]Institute of Molecular Genetics, Czech Academy of Sciences, Prague, Czech Republic.
*These authors contributed equally to this work.

Innovation

Despite the promise of targeted therapeutics, Her2^{high} breast cancer is still difficult to control. In this study, we show that Her2^{high} cells and tumors have increased respiratory supercomplex (SC) assembly, which can be selectively disrupted *in vitro* and *in vivo* by MitoTam, a mitochondrially targeted tamoxifen. This results in substantial reactive oxygen species generation in Her2^{high} background and efficient induction of apoptotic cell death. Hence, disruption of respiratory SCs in specific subsets of cancer cells represents a viable therapeutic strategy that avoids toxicity associated with conventional electron transport chain inhibitors. MitoTam has now passed preclinical testing and proceeds to phase I clinical trial.

Breast cancer is the prevailing type of neoplasia in women, and certain subtypes such as Her2^{high} breast carcinomas are difficult to treat (5, 6, 42). Her2 (also known as ErbB2) is a receptor tyrosine kinase that may regulate metabolism, for example, the pentose phosphate pathway (43). It has been suggested that a fraction of Her2 translocates into mitochondria, where it can affect bioenergetics (7). Tamoxifen, a mixed agonist/antagonist of the estrogen receptor (ER), is used as the first-line therapy in hormone-sensitive breast cancer, but is inefficient in the Her2^{high} disease. It was reported that tamoxifen inhibits mitochondrial complex I (CI), although at suprapharmacological doses (25). This inspired us to design, synthetize, and test tamoxifen tagged with the TPP$^+$ group, with expected accumulation adjacent to CI enhancing its effects on mitochondria.

In this study, we show that mitochondrially targeted tamoxifen (MitoTam) is far more efficient in killing breast cancer cells than the parental compound. In stark contrast to tamoxifen, MitoTam is highly effective toward cells and tumors with high level of Her2. This is linked to the elevated CI and increased SC assembly selectively disrupted by MitoTam, leading to enhanced reactive oxygen species (ROS) production and cell death. Interestingly, the sensitivity of Her2^{high} cells to MitoTam depends on the presence of Her2 in mitochondria at the IMM/matrix interface. We found that in a preclinical model, MitoTam almost completely cured Her2^{high} breast carcinomas without deleterious side effects, supporting the potential use of this novel ETC-targeted agent against Her2^{high} breast cancer highly recalcitrant to therapy (5).

Results

Tagging tamoxifen with TPP$^+$ leads to mitochondrial targeting and increased cell death

Tamoxifen, a low-affinity inhibitor of CI (25), was modified by the attachment of a TPP$^+$ group, which ensures mitochondrial accumulation based on the electrochemical gradient across the IMM. This TPP$^+$-modified tamoxifen, MitoTam (Fig. 1A), was labeled with fluorescein yielding MitoTam-F for intracellular visualization (Supplementary Fig. S1; Supplementary Data are available online at www.liebertpub.com/ars). Figure 1B shows that upon addition to MCF7 cells, MitoTam-F accumulates in the mitochondria, which become doughnut shaped and lose MitoTracker Far Red fluorescence. The enlarged color-balanced image of the intermediate state before the complete loss of red fluorescence shows green staining of internal structures of mitochondria, indicating that the accumulation of the drug at the IMM likely interferes with mitochondrial function. Figure 1C documents that MitoTam is more efficient in killing MCF7 cells than tamoxifen.

We estimated the IC_{50} value of MitoTam and tamoxifen for a number of breast cancer cell lines and found that in all cases, it was at least one order of magnitude lower for the TPP$^+$-tagged variant. On the other hand, IC_{50} values for noncancerous cell lines were more than one order of magnitude higher than for cancer cell lines, indicating a pharmaceutical window of opportunity (Table 1). As expected for a compound originating from an ER antagonist, MitoTam was found more efficient in killing the ER-positive MCF7 cells than their triple-negative counterparts, MDA-MB-231 cells (Fig. 1D). MitoTam also eliminated Her2^{high} ER-negative SKBR3 and MDA-MB-453 cells with high efficacy (Fig. 1E). Importantly, when the TPP$^+$ group of MitoTam was disabled by the removal of its positive charge, efficiency of the resulting compound (Tam-DPPO, for structure, see Supplementary Fig. S1) was greatly reduced (Fig. 1F). Similarly, the TPP-targeting group alone (Supplementary Fig. S1) had little effect (Fig. 1G). This illustrates the importance of mitochondrial targeting of the tamoxifen moiety for increased biological activity.

We next tested the effect of MitoTam on tamoxifen-resistant cells using MCF7 cells made resistant to tamoxifen by long-term exposure to escalating doses of the agent (TAM-R cells) (Fig. 1H). Figure 1I documents that TAM-R cells were slightly more susceptible to MitoTam. On the other hand, Tam-DPPO that lacks the delocalized cationic group was less efficient toward TAM-R cells than to parental MCF7 cells (Fig. 1J). We also attempted to prepare MitoTam-resistant MCF7 cells in a similar manner as we did for tamoxifen. However, we were not able to obtain any surviving population upon long-term culture (>6 months), suggesting that resistance to MitoTam may not develop, similarly as we documented before for MitoVES (33). Collectively, these data indicate that MitoTam exhibits superior structure-dependent killing activity that is not compromised in cells resistant to the parental compound.

MitoTam effectively kills cells with high levels of Her2 and efficiently suppresses Her2^{high} breast carcinomas

Breast cancer with high level of expression of the oncogene *HER2* is particularly difficult to manage. Therefore, we next investigated the effect of MitoTam on Her2^{high} breast cancer cells prepared by genetic manipulation. For this, we used MCF7 cells with relatively low level of Her2 and Her2-null MDA-MB-231 cells that were both transfected with Her2 plasmid to achieve Her2 expression levels similar to those found in natural Her2^{high} breast cancer cell lines (Fig. 2A). We also knocked down Her2 using shRNA in MCF7 cells, further reducing its level (Fig. 2A). As expected, MCF7 Her2^{high} cells were more resistant to tamoxifen than the parental cells (Fig. 2B). In stark contrast, Her2^{high} MCF7 and MDA-MB-231 cells were more susceptible to MitoTam than parental or Her2^{null} cells (Fig. 2C–E), while this preference was absent for Tam-DPPO (Fig. 2F).

Consistently with the higher level of cell death induction, MitoTam treatment resulted in stronger activation of the apoptotic pathway in MCF7 Her2^{high} cells compared with mock MCF7 cells (Fig. 2G). Western blotting (WB) revealed

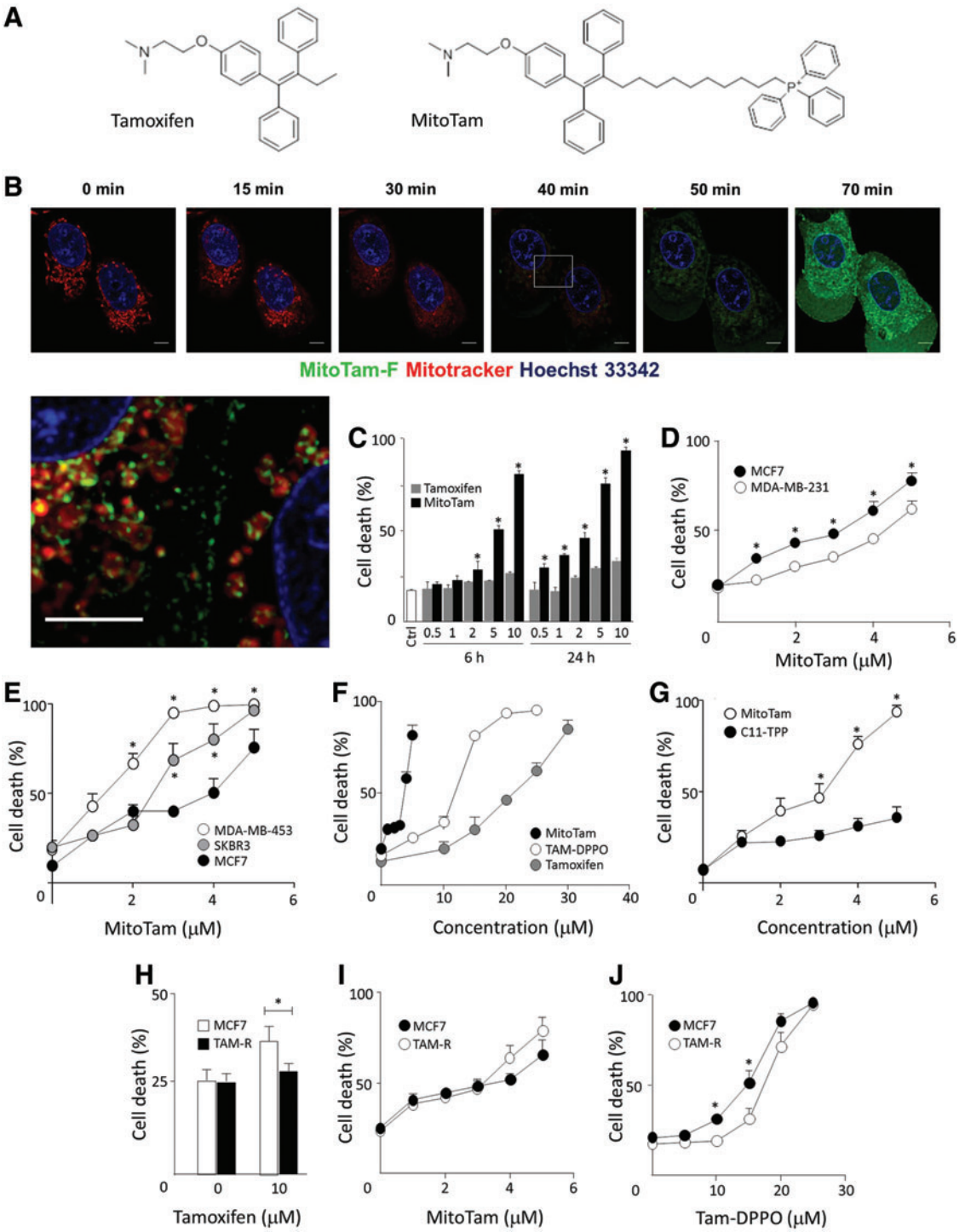

FIG. 1. MitoTam associates with mitochondria and efficiently kills breast cancer cells. **(A)** Structures of tamoxifen and tamoxifen tagged with the TPP^+ group (MitoTam). **(B)** MCF7 cells were preloaded with MitoTracker Far Red, exposed to FITC-labeled MitoTam (5 μM), and inspected by time-lapse confocal microscopy for the times shown. The *last panel* presents the magnified and color-balanced view of the region highlighted at 40-min time point. Size bar = 5 μm. **(C)** MCF7 cells were exposed to tamoxifen and MitoTam at the concentrations (μM) and time points shown, and cell death was evaluated using the Annexin V-FITC/PI method using flow cytometry. **(D)** MCF7 and MDA-MB-231 cells were exposed to MitoTam for 24 h at the concentrations shown and cell death was evaluated by Annexin V/PI. **(E)** MCF7, MDA-MB-453, and SKBR3 cells were exposed to MitoTam for 20 h at the concentrations shown and cell death was evaluated by Annexin V/PI staining. **(F)** MCF7 cells were exposed to MitoTam, Tam-DPPO, and tamoxifen or **(G)** MitoTam and C11-TPP for 24 h and cell death was evaluated by Annexin V/PI staining. **(H)** Parental and tamoxifen-resistant MCF7 cells (MCF7 and TAM-R cells, respectively) were exposed to tamoxifen, **(I)** MitoTam, or **(J)** Tam-DPPO for 24 h at the concentrations shown and cell death was evaluated by Annexin V/PI staining. Images in **(B)** are representative of three independent experiments; data in all other panels are mean values ($n \geq 3$) ± SEM. The symbol, *, indicates statistically significant difference ($p < 0.05$). TPP^+, triphenylphosphonium; Tam-DPPO, Diphenylphosphine oxide tamoxifen. To see this illustration in color, the reader is referred to the web version of this article at www.liebertpub.com/ars

Table 1. IC_{50} Values for Killing of Breast Cancer Cell Lines and Nonmalignant Cells with Tamoxifen and MitoTam

Cell line[a]	*IC_{50} (tamoxifen)*[b]	*IC_{50} (MitoTam)*
BT474	29.8	2.4
MCF7	15.2	1.25
MCF7 Her2^{high}	21.6	0.65
MCF7 Her2^{low}	14.1	1.45
MDA-MB-231	35.8	6.2
MDA-MB-436	12.6	3.4
MDA-MB-453	17.5	2.5
SK-BR-3	28.3	3.5
T47D	17.3	3.4
NeuTL	35.6	4.5
EAhy926[c]	40.3	10.9
A014578	n.d.	55.9
H9c2	n.d.	48.4

[a]Cells were treated at ~60% confluence.
[b]The IC_{50} values were derived from viability curves using crystal violet staining and are expressed in μM.
[c]EAhy926 cells were evaluated for the effect of MitoTam after reaching complete confluence.
n.d., not determined.

accelerated cleavage of procaspase-9 and Parp1/2 in Her2^{high} cells, as well as an increase of proapoptotic Bax and decrease of the antiapoptotic Bcl-2 protein. Interestingly, the level of Her2 decreased in MCF7 Her2^{high} cells upon exposure to MitoTam. In a colony-forming assay, tamoxifen was proficient in suppressing formation of colonies in MCF7 and MCF7 mock cultures (Fig. 2H), while MitoTam was more efficient in MCF7 Her2^{high} cultures, corroborating anticancer efficacy of MitoTam against Her2^{high} breast cancer. Finally, MitoTam showed an additive effect with inhibitors of Her2 signaling in Her2^{high}, but not in parental MCF7 cells (Fig. 2I, J), indicating that MitoTam targets sites or pathways distinct from canonical Her2 signaling. In summary, these results show that high Her2 expression is associated with increased sensitivity to MitoTam.

To see whether Her2 sensitizes breast tumors to MitoTam *in vivo*, we used the FVB/N *c-neu* mouse strain subcutaneously (s.c.) injected with NeuTL cells derived from spontaneous Her2^{high} breast carcinoma (13). Figure 3A (and Supplementary Fig. S2A with representative images) documents a strong effect of MitoTam (0.54 μmol/mouse/dose), inhibiting growth of syngeneic tumors by ~80%, while tamoxifen (applied at 2.69 μmol/mouse/dose, that is, at ~5-times higher dose than MitoTam) was much less efficient.

We next tested another tumor model, in which Balb/c nude mice were s.c. injected with MCF7 mock or MCF7 Her2^{high} cells. Tamoxifen, which had a modest effect on parental MCF7 mock tumors (2 μmol/mouse/dose), was even less efficient in suppressing Her2^{high} carcinomas, where it did not prevent reaching the ethical endpoint (Fig. 3B and Supplementary Fig. S2C, D). On the other hand, MitoTam at 8 times lower dose (0.25 μmol/mouse/dose) prevented reaching the ethical endpoint in all situations (Supplementary Fig. S2C, D). It slowed down the growth of MCF7 mock tumors (featuring relatively low level of Her2) and, after two doses, tumor progression stopped (Fig. 3B).

Most importantly, MitoTam suppressed Her2^{high} carcinomas such that their volume decreased threefold from the original size with complete disappearance in two of the treated animals (Fig. 3B and Supplementary Fig. S2B with representative images). These animals stayed tumor free for 8 months following cessation of MitoTam administration, indicating complete eradication of the Her2^{high} breast carcinomas in these particular cases. Immunohistochemistry analysis of control and treated tumors document increased TUNEL-positive cells, in particular in Her2^{high} tumors (Fig. 3C). This is supported by WB showing high level of procaspase-9 cleavage in MitoTam-treated Her2^{high} tumors, increased Bax, and decreased Bcl-2 protein levels. WB also documents high level of the Her2 protein in Her2^{high} tumors and its decrease upon MitoTam treatment (Fig. 3D).

MitoTam effectively suppressed tumors induced by mammary expression of the *HER2* transgene in FVB/N *c-neu* mice (13) (Fig. 3E and Supplementary Fig. S2E), demonstrating effectiveness in a more natural situation where a tumor appears in its native environment, without the initial presence of homogeneous Her2^{high} cell population. MitoTam also reduced invasiveness in a zone exclusion assay (Supplementary Fig. S3A) and was effective in the Her2^{high} mammosphere model (Supplementary Fig. S3B) that generates cells with cancer stem-like properties resistant to conventional therapy (12, 49). In addition, MitoTam, but not tamoxifen, interfered with sphere formation in this situation (Supplementary Fig. S3C, D). Importantly, MitoTam suppressed not only the primary tumor growth (Fig. 3F and Supplementary Fig. S2F), but also the metastatic burden in blood, lung, and liver (Fig. 3G) in the experimental 4T1 model of Her2^{high} metastatic breast carcinoma in Balb/c mice.

Collectively, these data clearly demonstrate that MitoTam efficiently suppresses growth and progression of Her2^{high} carcinomas.

MitoTam induces ROS, dissipates mitochondrial potential, and suppresses mitochondrial respiration via *complex I*

Since MitoTam showed efficacy superior to that of tamoxifen, in particular in suppressing Her2^{high} tumors, we further investigated its mode of action. We first tested its effect on generation of ROS as mitochondrial targeting can improve the efficacy of ROS generation (9, 10, 37). Clearly, MitoTam induced ROS within a short period of treatment, while no ROS was induced with tamoxifen even at much higher doses. The effect of MitoTam was more profound for Her2^{high} cells (Fig. 4A) when mitochondrial ROS-specific probe (MitoSOX) was used. This was linked to cell death induction since the ROS scavenger, N-acetyl cysteine (NAC), suppressed the killing activity of the agent (Fig. 4B).

We next tested the effect of MitoTam on $\Delta\Psi_{m,i}$. Using confocal microscopy and flow cytometry with TMRM probe, we found that MitoTam was very efficient in $\Delta\Psi_{m,i}$ dissipation, while tamoxifen had no effect (Fig. 4C, D). $\Delta\Psi_{m,i}$ is important for ROS generation in response to MitoTam and in cell death induction by the agent as pretreatment with the uncoupler FCCP suppressed both events (Fig. 4E, F). Interestingly, MCF7 Her2^{low} cells showed higher basal $\Delta\Psi_{m,i}$, although this was not followed by increased activity of MitoTam. Finally, we show that MitoTam, in contrast to tamoxifen, decreased $\Delta\Psi_{m,i}$ almost to the same level as FCCP (Fig. 4G). These data support the notion that ROS generation

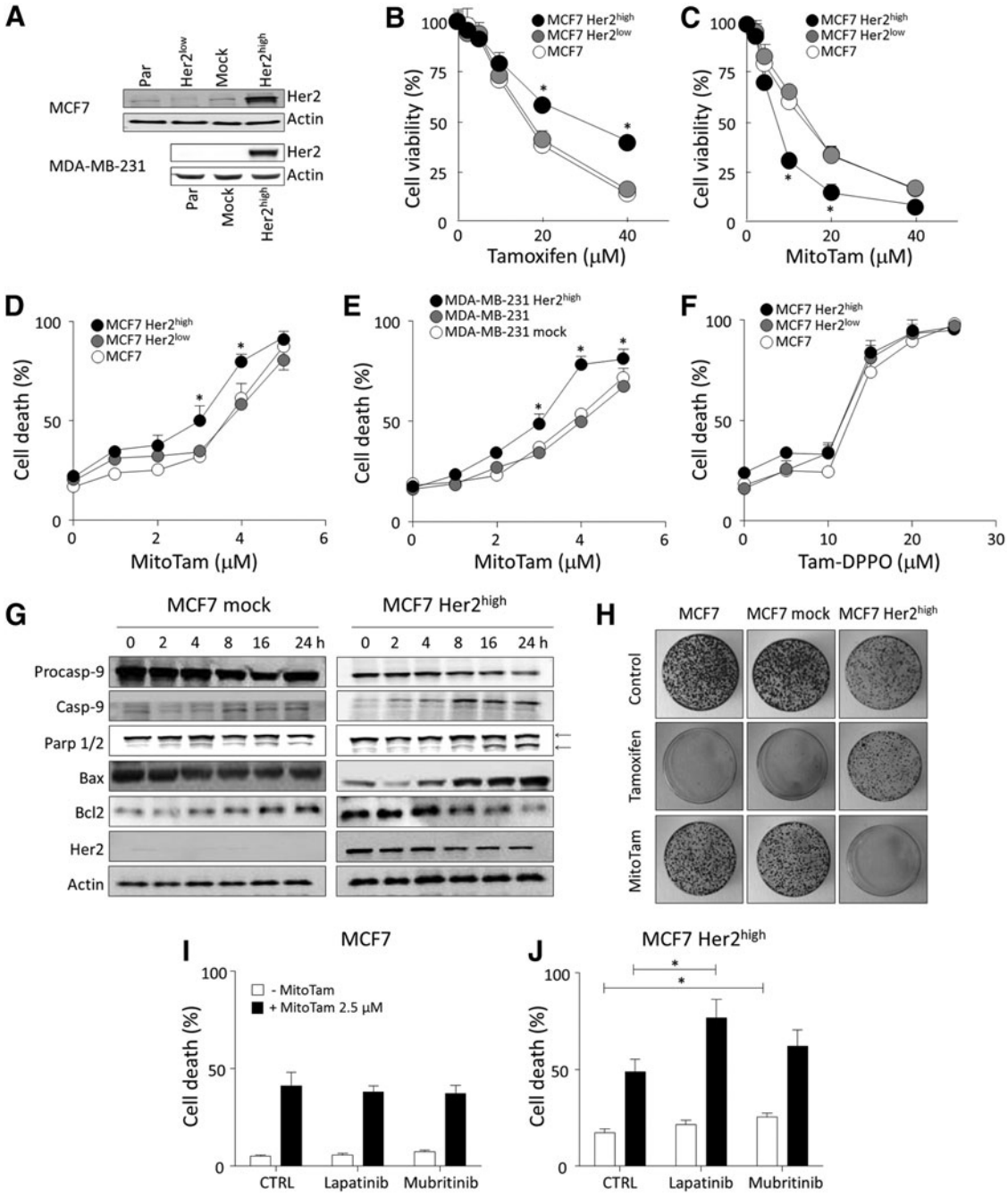

FIG. 2. MitoTam is more efficient in killing Her2^{high} cells than their Her2^{low} counterparts. **(A)** MCF7 parental, Her2^{low} (shRNA transfected), mock (empty plasmid transfected), and Her2^{high} cells (Her2 plasmid transfected) and MDA-MB-231 parental, mock, and Her2^{high} cells were assessed for the Her2 protein in whole cell lysate using WB with actin as a loading control. MCF7, MCF7 Her2^{low}, and MCF7 Her2^{high} cells were exposed to **(B)** tamoxifen or **(C)** MitoTam at the concentrations shown for 16 h and cell viability assessed using the crystal violet method. **(D)** MCF7, MCF7 Her2^{low}, and MCF7 Her2^{high} cells and **(E)** MDA-MB-231, MDA-MB-231 mock, and MDA-MB-231 Her2^{high} cells were exposed to MitoTam at the concentrations shown for 24 h, and cell death was evaluated using Annexin V/PI staining. **(F)** MCF7, MCF7 Her2^{low}, and MCF7 Her2^{high} cells were exposed to TAM-DPPO at the concentrations shown for 24 h and cell death was evaluated using Annexin V/PI staining. **(G)** MCF7 mock and MCF7 Her2^{high} cells were exposed to 2.5 μM MitoTam for the times shown and the levels of procaspase-9, caspase-9, Parp 1/2 (both the intact and cleaved forms, indicated by *arrows*), Bax, Bcl2, and Her2, with actin as loading control, were estimated by WB. **(H)** MCF7, MCF7 mock, and MCF7 Her2^{high} cells were seeded in Petri dishes in soft agar, cultured for 14 days after 16-h treatment with 20 μM tamoxifen or 2.5 μM MitoTam, and stained with crystal violet to visualize individual colonies. **(I)** MCF7 and **(J)** MCF7 Her2^{high} cells were exposed to 2.5 μM MitoTam or solvent control in the presence of lapatinib (0.5 μM) or mubritinib (0.5 μM) for 24 h and cell death was evaluated. Images in **(A)**, **(G)**, and **(H)** are representative of three independent experiments. Data in all other panels are mean values ($n \geq 3$) ± SEM. The symbol, *, indicates statistically significant differences ($p < 0.05$).

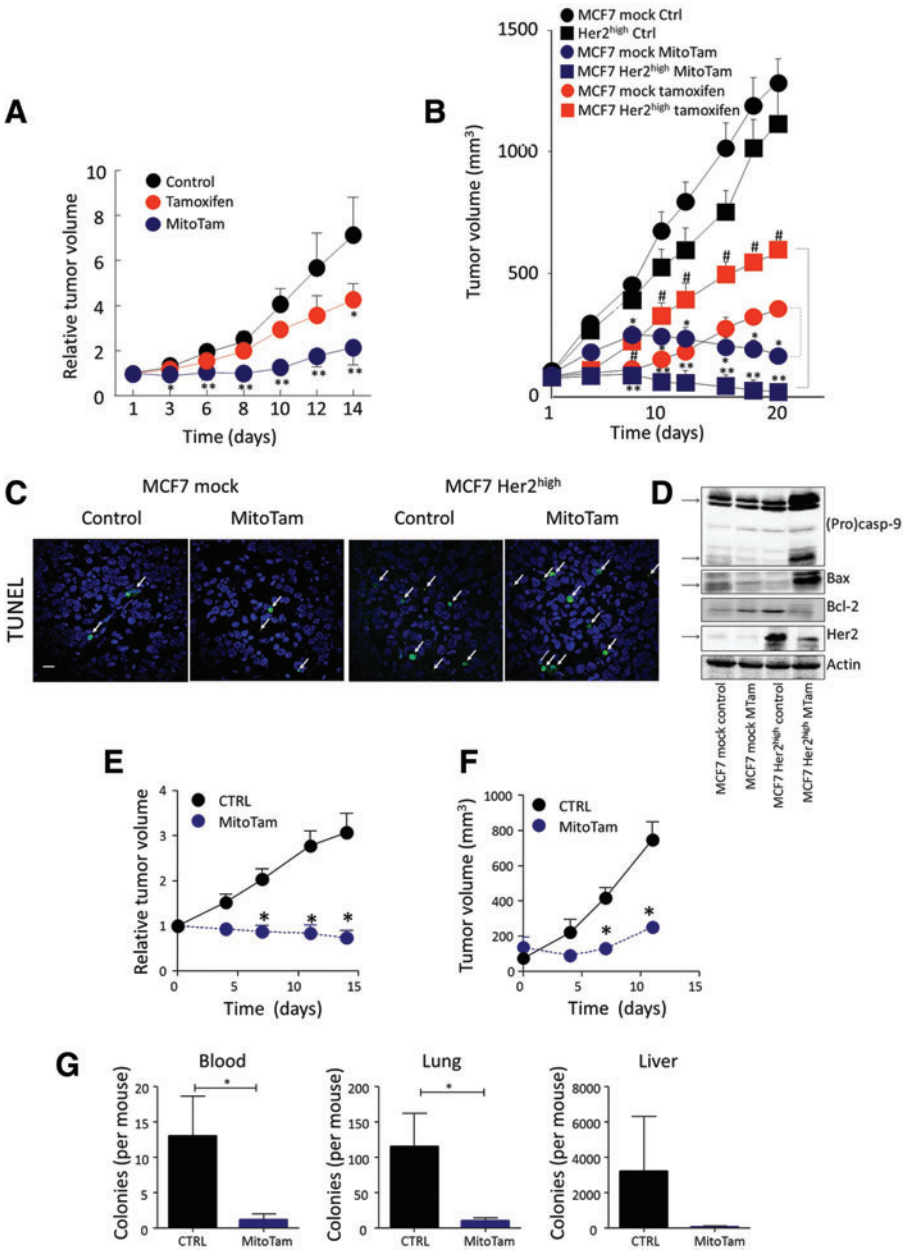

FIG. 3. MitoTam efficiently suppresses Her2^{high} breast carcinomas. (A) FVB/N *c-neu* mice s.c. injected with syngeneic NeuTL cells (2×10^6 cells per animal) were treated twice a week with tamoxifen (2.69 μmol/mouse/dose) or MitoTam (0.54 μmol/mouse/dose) dissolved in 4% EtOH in corn oil, 100 μl per dose, and tumor volume evaluated by USI. **(B)** Balb-c *nu/nu* mice were implanted with a slow-release estradiol pellet and injected s.c. with 2×10^6 MCF7 mock or MCF7 Her2^{high} cells per animal. As soon as USI-detectable tumors appeared ($\sim$50 mm^3), the mice were treated with i.p. injection with 100 μl of tamoxifen (2 μmol/mouse/dose) or MitoTam (0.25 μmol/mouse/dose) dissolved in 4% EtOH in corn oil on days 3 and 7 of every week, and tumor volume was visualized and evaluated using USI. **(C)** Control and MitoTam-treated MCF7 mock and MCF7 Her2^{high} cell-derived tumors, excised at the end of the experiment, were fixed, paraffin embedded, and stained using the TUNEL technique. The *arrows* indicate TUNEL-positive cells. Size bar = 50 μm. **(D)** Control and treated tumors as shown in **(B)** were lysed and evaluated for the level of procaspase-9, caspase-9, Bax, Bcl-2, and Her2 with actin as loading control using WB. **(E)** FVB/N *c-neu* mice with spontaneous tumors were treated twice a week with MitoTam (0.54 μmol/mouse/dose) or solvent control, and tumor volume was evaluated. **(F)** Balb/c mice were s.c. injected with syngeneic 4T1 cells (1×10^6 cells per animal) and treated with MitoTam (0.25 μmol/mouse/dose) or solvent control twice a week, and tumor volume was evaluated. **(G)** Blood, lung, and liver harvested from animals in **(F)** were homogenized and subjected to selection in the presence of 6-thioguanine for 10 days and colonies were counted. Data in **(A)** and **(B)** are mean values ($n=6$) ± SEM and, in **(E)** and **(F)**, are mean values ($n\geq5$) ± SEM. The symbols, *, **, and #, indicate statistically significant differences ($p<0.05$). WB, Western blotting. To see this illustration in color, the reader is referred to the web version of this article at www.liebertpub.com/ars

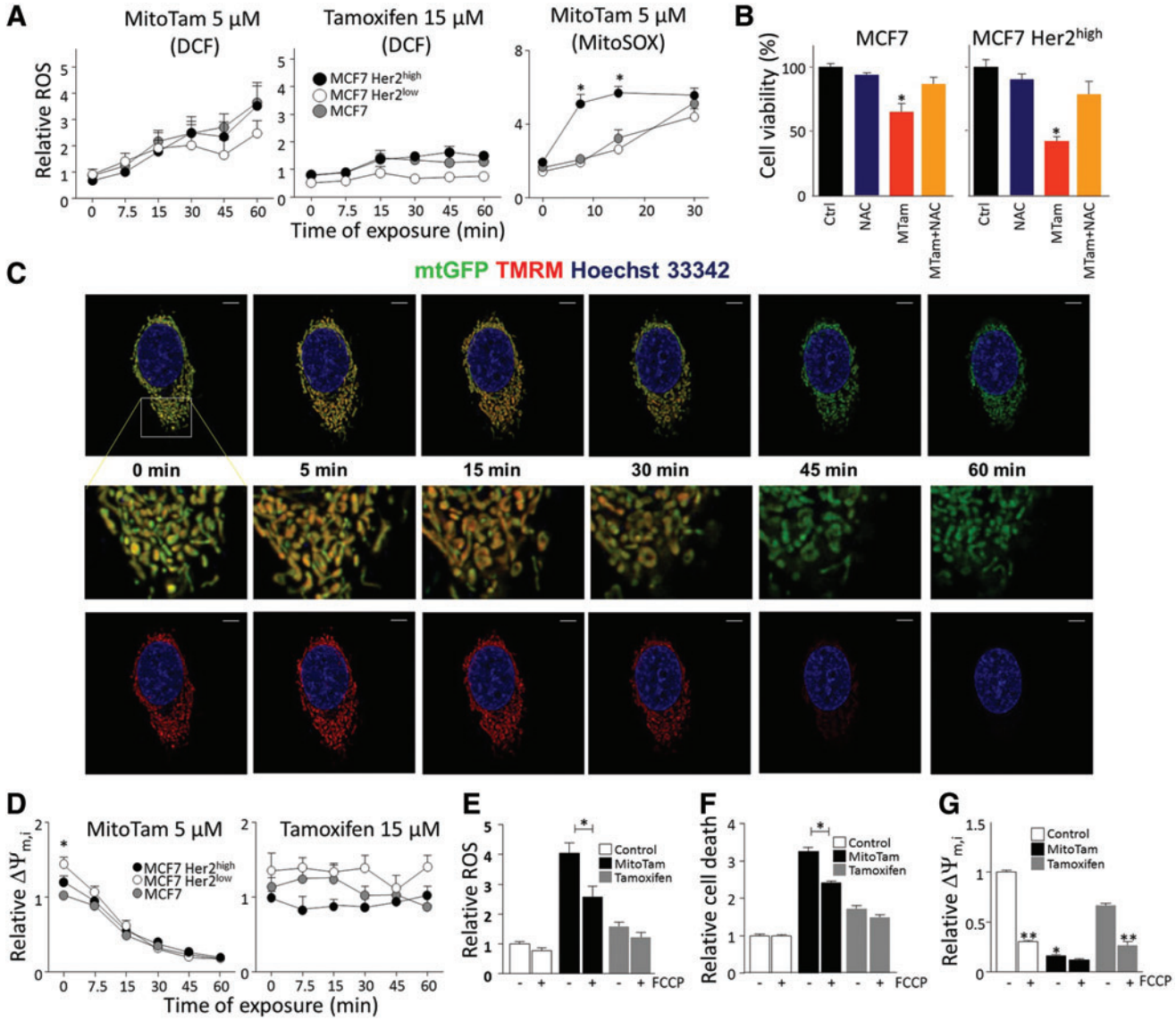

FIG. 4. MitoTam induces generation of ROS and dissipation of $\Delta\Psi_{m,i}$. **(A)** MCF7, MCF7 Her2^{low}, and MCF7 Her2^{high} cells exposed to 5 μM MitoTam and 15 μM tamoxifen were assessed for ROS using DCF or MitoSOX. **(B)** Cells were pretreated with 10 μM NAC, exposed to 2.5 μM MitoTam for 24 h, and evaluated for viability. **(C)** MCF7 Her2^{high} cells were stably transfected with mtGFP, preloaded with TMRM, and exposed to 5 μM MitoTam, followed by time-lapse confocal microscopy. Size bar = 5 μm. **(D)** Cell lines exposed to 5 μM MitoTam and 15 μM tamoxifen were assessed for $\Delta\Psi_{m,i}$ using TMRM. **(E)** MCF7 cells exposed to 10 μM MitoTam or 30 μM tamoxifen in the absence or presence of 10 μM FCCP were assessed for ROS using DCF (60-min treatment) or **(F)** cell death (4-h treatment). **(G)** MCF7 cells, control or exposed to 10 μM MitoTam or 30 μM tamoxifen for 60 min, were evaluated for $\Delta\Psi_{m,i}$ in the absence or presence of 10 μM FCCP. The symbol, *, indicates statistically significant differences ($p < 0.05$) between MCF7 Her2^{high} and MCF7/MCF7 Her2^{low} cells/tumors **(A, D)**, cells treated in the absence and presence of NAC **(B)**, or MitoTam **(G)**. The symbol, **, indicates statistically significant difference in the absence and presence of FCCP **(G)**. FCCP, carbonyl cyanide 4-(trifluoromethoxy)phenylhydrazone; NAC, N-acetyl cysteine; ROS, reactive oxygen species. To see this illustration in color, the reader is referred to the web version of this article at www.liebertpub.com/ars

is mediating the killing activity of MitoTam and that this is more profound in Her2^{high} cells.

Since MitoTam is targeted to mitochondria (more specifically to the interface of the IMM and matrix), we tested its effect on mitochondrial respiration. Using high-resolution respirometry, we found that MitoTam suppressed CI-dependent respiration more efficiently than CII-dependent respiration and that this effect was stronger for MitoTam than for tamoxifen (Fig. 5A, B, and Table 2). In addition, MitoTam inhibited NADH-cytochrome c (CI-CIII), but not succinate-cytochrome c (CII-CIII) oxidoreductase activity in MCF7 cells (Fig. 5C, D), suggesting that CI is the likely target. To support a role of CI in the anticancer activity of MitoTam, we used Chinese hamster lung fibroblast cells with functional and mutant CI (46) transformed with H-Ras (8). Interestingly, the CI dysfunctional B10$_{H\text{-}Ras}$ cells (Fig. 5E) were more resistant to MitoTam than the parental B1$_{H\text{-}Ras}$ cells (Fig. 5F).

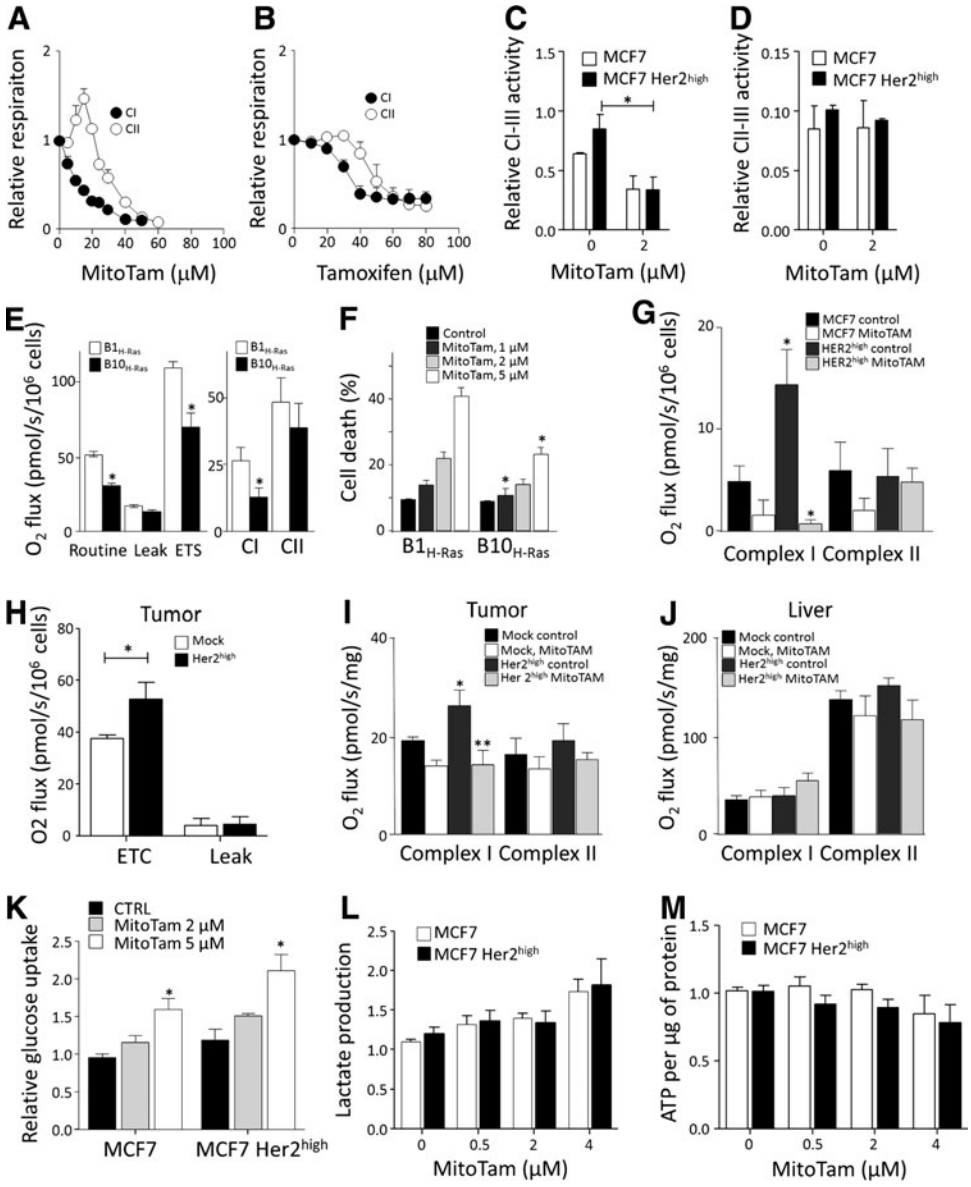

FIG. 5. Respiration is elevated in Her2^{high} cells and tumors and is efficiently suppressed by MitoTam. MCF7 cell respiration (10^6 cells/ml) was evaluated in the presence of CI (glutamate/malate) and CII substrate (succinate) with titrated **(A)** MitoTam or **(B)** tamoxifen. **(C)** NADH-cytochrome c (CI-CIII) and **(D)** succinate-cytochrome c (CII-CIII) oxidoreductase activity was measured in mitochondria isolated from MCF7 and MCF7 Her2^{high} cells and corrected for citrate synthase. **(E)** $B1_{H\text{-}Ras}$ and $B10_{H\text{-}Ras}$ cells were evaluated for routine, leak, and ETS respiration and respiration *via* CI and CII, and **(F)** for cell death upon exposure to MitoTam for 12 h. **(G)** MCF7 and MCF7 Her2^{high} cells were treated with 2.5 μM MitoTam for 1 h, harvested, and evaluated for respiration *via* CI and CII. **(H)** MCF7 mock and MCF7 Her2^{high} tumors were evaluated for ETC and leak respiration and **(I)** CI and CII respiration. **(J)** Liver from the same control and MitoTam-treated mice as in **(I)** were evaluated for CI and CII respiration. **(K)** Glucose uptake in MCF7 and MCF7 Her2^{high} cells was measured after 1-h incubation with MitoTam (2 μM and 5 μM) or solvent control. **(L)** Lactate production and **(M)** ATP level and were measured in MCF7 and MCF7 Her2^{high} cells after incubation with MitoTam (5 μM) for the times indicated. The symbols, * and **, indicate statistically significant differences ($p < 0.05$).

We next tested MCF7 cells and their Her2^{high} counterparts for respiration and found that the latter respired more, in particular *via* CI (Fig. 5G). In addition, the CI-CIII activity was higher in mitochondria from Her2^{high} cells (Fig. 5C). We also found that MitoTam suppressed respiration of Her2^{high} cells more profoundly than that of parental MCF7 cells (Fig. 5G). In this case, we used a different setup than that used in Figure 5A and B. Rather than titrating cells placed in the respirometer chamber with MitoTam, they were cultured with the agent for 1 h, after which respiration was assessed.

The *in vitro* results were recapitulated by assessing *in vivo* effects of MitoTam (*c.f.* Fig. 3B). Tumors derived from Her2^{high} cells had unchanged leak respiration, but increased maximal respiratory capacity (Fig. 5H) and higher CI-dependent respiration (Fig. 5I), which was strongly suppressed in response to MitoTam treatment of the animals, while

Table 2. Inhibition of Respiration *via* Complex I and Complex II

Complex	*IC_{50} (tamoxifen)*[a]	*IC_{50} (MitoTam)*
CI	30	11.5
CII	47.2	30.6

[a]IC_{50} values were estimated from the inhibition of respiration of MCF7 cells grown to 60–70% confluence in the Oxygraph using the CI (glutamate/malate) and CII substrates (succinate) under increasing concentration of tamoxifen or MitoTam.

CII-dependent respiration was unchanged (Fig. 5I). These effects were tumor specific as there was no difference in respiration and no effect of MitoTam in the liver tissue from the same animals (Fig. 5J).

Concerning glycolysis, neither glucose uptake (Fig. 5K) nor lactate production (Fig. 5L) and ATP levels (Fig. 5M) were affected differentially in parental and Her2^{high} cells by MitoTam. This suggests that alteration in glycolytic compensation is not responsible for increased sensitivity of Her2^{high} cells to MitoTam.

Collectively, these data document that MitoTam suppresses respiration *via* CI both in cultured cells *in vitro* and in breast carcinomas *in vivo*, resulting in ROS generation and cell death.

MitoTam disrupts respiratory SCs elevated in Her2^{high} cells and tumors

The increased respiration of Her2^{high} cells *via* CI might be related to a more efficient assembly of respiratory complexes (RCs). We therefore evaluated MCF7 Her2^{high} and MCF7 mock cells for expression of components of mitochondrial RCs using WB. Of these, subunits of CI and, to some extent, those of CIII and CIV were more expressed (Fig. 6A). The level of respiratory SCs, including the respirasome, an SC comprising CI, CIII, and CIV (1, 2), was also increased in MCF7 Her2^{high} cells, as determined by native blue gel electrophoresis (NBGE) (Fig. 6B, D). Interestingly, treatment of MCF7 Her2^{high} cells with MitoTam disrupted the SC (Fig. 6C, E) in the Her2^{high} background.

To see if MCF7 cells and their Her2^{high} counterparts maintain these features also *in vivo*, we analyzed tumors from control and MitoTam-treated mice. NBGE analysis documents that tumors derived from MCF7 Her2^{high} cells contain higher level of SCs than tumors derived from parental cells and that the respirasome was disrupted by MitoTam treatment in the Her2^{high} situation (Fig. 6F, H). This effect was not secondary to the suppression of individual protein subunits of ETC complexes as no change in expression of these subunits was detected by WB after SDS-PAGE in tumors from MitoTam-treated and control mice (Fig. 6G). These data suggest that MitoTam directly disrupts respiration *via* CI and the respirasome, an effect that is much more prominent in Her2-high cells.

To gain insight into the interaction of MitoTam with CI, we performed molecular modeling of MitoTam association with CI, using the recently published crystal structure of *Yarrowia lipolytica* CI resolved at 3.6–3.9 Å (60). Among the 20 poses with predicted highest binding affinity, we identified 3 preferred binding regions: inside the ubiquinone (UbQ)-binding pocket, at its entrance, and at the surface of the transmembrane region of the P_P module. The internal poses share the same binding cavity as well as orientation of the tamoxifen moiety with the predicted position of UbQ (Fig. 7), while the external poses are in close proximity to the cavity's entrance. This suggests that MitoTam could affect UbQ interaction with CI and in this way stimulate ROS generation, consistent with observed experimental results.

Her2 is localized at the IMM

The Her2 protein was recently shown to localize also into mitochondria using GFP-tagged Her2 fragments and biochemical means (7), but this unexpected report has not been confirmed. We therefore studied localization of Her2 in our cellular models using several approaches. STED confocal microscopy of MCF7 Her2^{high} cells revealed colocalization of a fraction of the Her2 protein with the IMM protein ATP synthase. As expected, Her2 was also detected in the cytoplasm and on the plasma membrane (Fig. 8A). This is consistent with WB of fractionated cells, showing high levels of Her2 in mitochondria in MCF7 Her2^{high} cells as well as in a number of other breast cancer cell lines (Fig. 8B).

We then performed immunogold transmission electron microscopy (IG-TEM). Figure 8C reveals that MCF7 Her2^{high} cells contain more Her2 than their parental counterparts at the IMM (light blue arrowheads) and that some Her2 signal is also associated with stress fibers in the cytoplasm (green arrowheads). The super-resolution Biplane FPALM/dSTORM technique (Fig. 8D) documents that in MCF7 Her2^{high} cells, Her2 is primarily associated with the outer surface of the mitochondrial matrix mtHsp70-stained region, highly indicative of localization at the IMM. This was

FIG. 6. Increased supercomplex assembly in Her2^{high} cells and tumors is disrupted by MitoTam. (A) Whole cell lysate from MCF7 mock and MCF7 Her2^{high} cells was assessed for the expression of subunits of CI, CII, CIII, CIV, and CV as shown using SDS-PAGE, followed by WB, with actin as loading control. **(B)** Mitochondrial fraction was probed for respiratory complexes and SCs by WB following NBGE with the following antibodies: CI, NDUFA9; CII, SDHA; CIII, Core I; CIV, Cox5a; and CV, ATPβ; Hsp60 was used as loading control. **(C)** MCF7 mock and MCF7 Her2^{high} cells were exposed to 2.5 μM MitoTam for the time periods indicated, and isolated mitochondrial fractions were evaluated for the CI complex and SC by WB following NBGE. **(D)** Densitometric evaluation of NBGE blots shown in **(B)**. **(E)** Densitometric evaluation of NBGE blots shown in **(C)**. **(F)** Control and MitoTam-treated tumors derived from MCF7 mock and MCF7 Her2^{high} cells were evaluated for complexes and SCs as described above for **(B)**. **(G)** Control and MitoTam-treated tumors derived from MCF7 mock and MCF7 Her2^{high} cells were homogenized and evaluated for subunits of mitochondrial complexes by WB following SDS-PAGE with actin as loading control. **(H)** Densitometric evaluation of NBGE blots shown in **(F)**. Images **(A–C, F, and G)** are representative of 3 independent experiments. Data (**D**, **E, H**) are mean values ± SEM from three independent experiments. NBGE, native blue gel electrophoresis.

further documented by WB analysis of submitochondrial fractions, where Her2 was detected in intact mitochondria and isolated mitoplasts, but not in the intermembrane space (IMS) and outer mitochondrial membrane (OMM) fractions (Fig. 8E). Moreover, using the protease protection assay, Her2 remained unchanged upon addition of trypsin to intact mitochondria isolated from MCF7 Her2^{high} cells, while the OMM marker, VDAC, was almost completely digested; both proteins were sensitive to trypsin treatment in mitochondria solubilized with Triton-X100 (Fig. 8F).

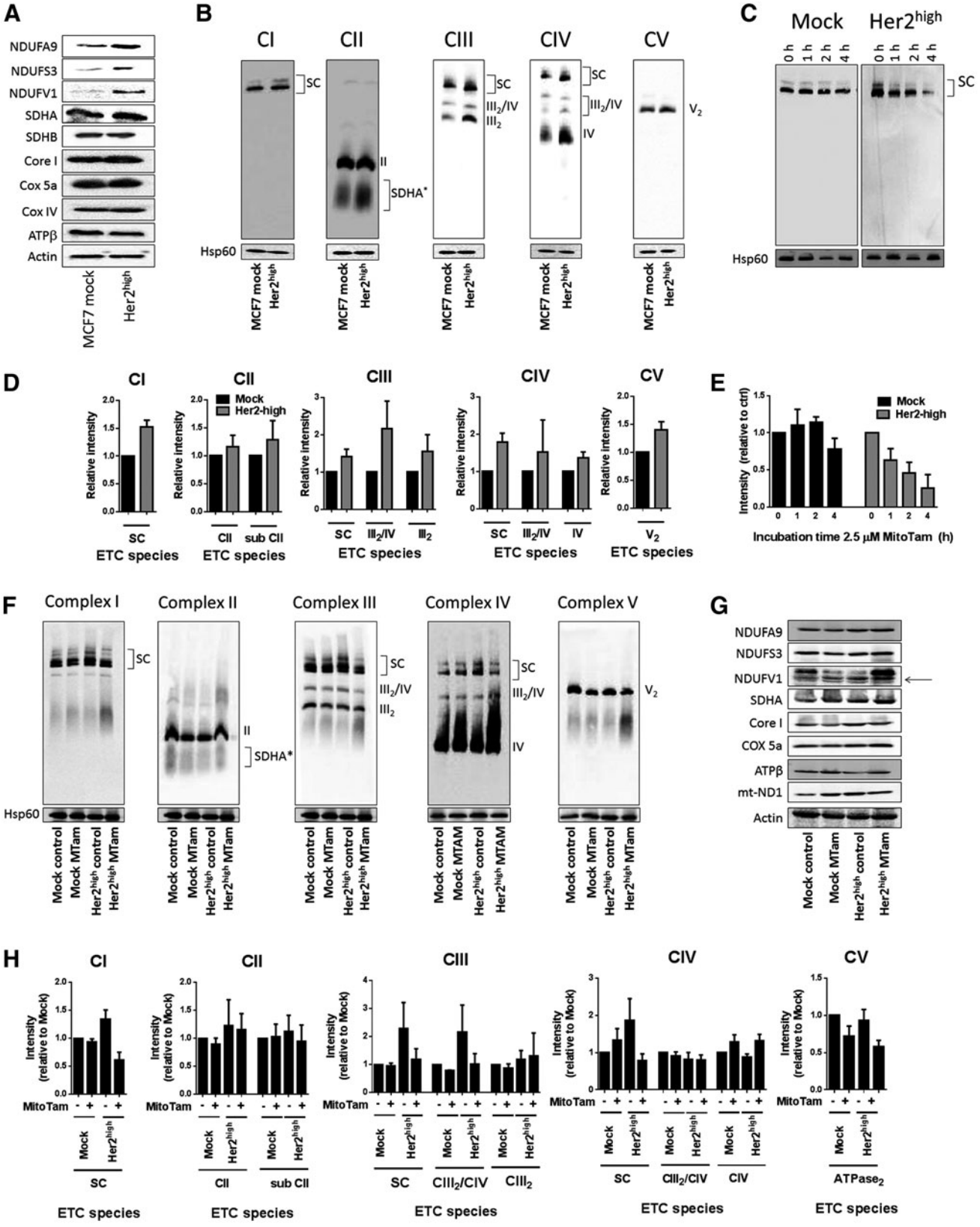

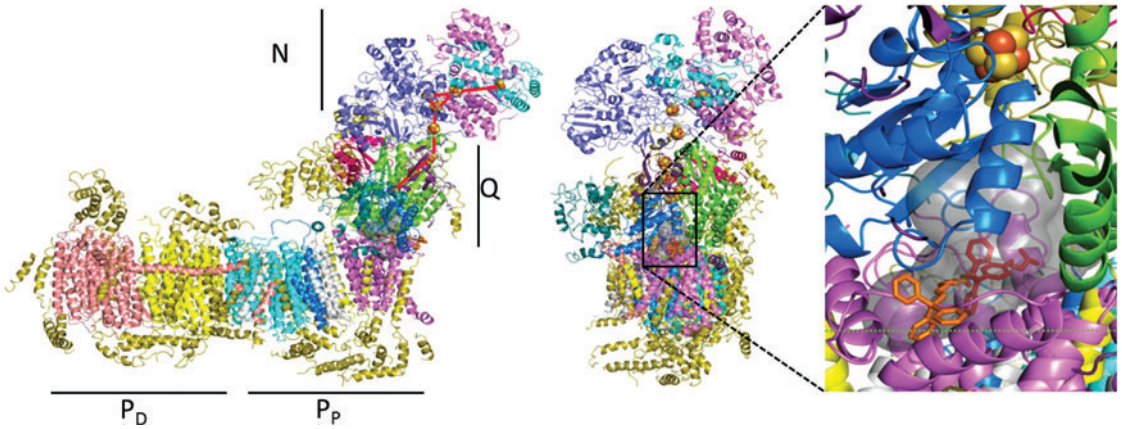

FIG. 7. Molecular modeling of MitoTam interaction with complex I. *Left*: Molecular structure of complex I with indicated N, Q, P_D, and P_P modules. The broken *red* line indicates movement of electrons from the catalytic center of CI to their acceptor, UbQ. *Right*: The structure of CI is shown using its lateral views with the *boxed area* containing the cavity into which MitoTam can bind. The *boxed area* is enlarged, indicating two most probable positions of MitoTam inside the cavity, with the potential effect on electron flow. UbQ, ubiquinone. To see this illustration in color, the reader is referred to the web version of this article at www.liebertpub.com/ars

We also fractionated MCF7 and MCF7 $Her2^{high}$ cell-derived tumors treated with MitoTam and assessed them for Her2 (Fig. 8G). Consistently with cultured cells, Her2 was present primarily in the mitochondrial fraction of $Her2^{high}$ tumors. Collectively, these findings confirm mitochondrial localization of Her2 and document its presence at the IMM.

Mitochondrial Her2 determines susceptibility to MitoTam

We speculated that the fraction of Her2 in mitochondria may promote the increased sensitivity of $Her2^{high}$ MCF7 cells to MitoTam. According to a recent report, mtHsp70 is needed for mitochondrial localization of Her2 (7), and we also detected Her2-mtHsp70 interaction using immunoprecipitation (Fig. 9A). We knocked down mtHsp70 in MCF7 cells by siRNA (Fig. 9B) and this reduced MitoTam-induced cell death selectively in MCF7 $Her2^{high}$ cells, while having no effect in mock-transfected or $Her2^{low}$ cells, completely abrogating the increased sensitivity of $Her2^{high}$ cells to MitoTam (Fig. 9C). Cells transfected with mtHsp70 siRNA showed lower levels of Her2, mtHsp70, and NDUFA9 in whole cell lysate (Fig. 9D) and, in particular, in the mitochondrial fraction (Fig. 9E). NBGE also documents reduced SC levels in mtHsp70 knockdown cells using an antibody to CI and CIII subunits, while no effect on CII was observed (Fig. 9F).

To evaluate the involvement of mitochondrial Her2 in the susceptibility of $Her2^{high}$ cells to MitoTam, we used a set of modified Her2 constructs with increased or decreased ability to translocate to mitochondria. Upon transient transfection in MCF7 cells, the construct comprising Her2 tagged with the mitochondrial targeting sequence of Cox8 (MTS) made the cells more susceptible to MitoTam than the construct where the inner MTS of Her2, described earlier (7), was deleted (ΔMTS) (Fig. 9G). The insert in Figure 9G shows different

FIG. 8. Her2 is localized at the inner mitochondrial membrane. (A) MCF7 $Her2^{high}$ cells stained using anti-ATPβ IgG, followed by Alexa Fluor 488-stained secondary IgG, and anti-Her2 IgG, followed by Alexa Fluor 555 secondary IgG, were inspected by STED confocal microscopy. *White arrows* show colocalization of anti-ATPβ and anti-Her2 signals. Size bar = 5 μm. **(B)** Breast cancer cell lines as shown were fractionated into the cytosolic + plasma membrane fraction and the mitochondrial fraction and assessed for the level of Her2 by WB following SDS-PAGE. Mitochondrial marker, COXIV, and cytosolic markers, SOD1 and actin, were used as loading controls. **(C)** MCF7 and MCF7 $Her2^{high}$ cells were assessed for localization of Her2 using IG-TEM. The light *blue arrowheads* show position of gold particles associated with Her2 in mitochondria, the *green* ones outside mitochondria, often pointing to stress fibers. Size bar = 0.5 μm. The two images on the *right-hand* side are enlarged *boxed* regions in the *middle* images. **(D)** MCF7 $Her2^{high}$ cells were subjected to double-staining with anti-Her2 IgG, followed by Alexa Fluor 647-stained secondary IgG, and anti-mtHsp70 IgG, followed by Cy3b-stained secondary IgG, and inspected using the super-resolution PALM microscopy. The *left* and *bottom images* are enlarged *boxed* images in the *top right-hand* micrograph. Size bar = 10 μm. **(E)** MCF7 $Her2^{high}$ cell lysate, their cytosolic + plasma membrane fraction (C+PMF), mitochondria, mitoplasts, and intermembrane space + outer membrane (IMS+OMM) fraction were assessed for Her2 using WB after SDS-PAGE with actin, NDUFA9, VDAC, Cyt c, and SDHA as loading controls and preparation markers. **(F)** Mitochondrial fraction of MCF7 $Her2^{high}$ cells was exposed to trypsin in the absence or presence of Triton X-100 for the periods indicated, at which time the preparations were assessed for Her2 by WB following SDS-PAGE. VDAC, ATPβ, NDUFS3, COXIV, and Cyt c were used as markers of different mitochondrial compartments. **(G)** Cytosolic + plasma membrane fraction and mitochondria of MCF7 mock or MCF7 $Her2^{high}$ tumors, excised from either control or MitoTam-exposed mice, were evaluated for Her2 by WB following SDS-PAGE with COXIV and actin as fraction markers and loading controls. All images represent at least three independent experiments. To see this illustration in color, the reader is referred to the web version of this article at www.liebertpub.com/ars

levels of mitochondrial Her2 expression in MTS- and *Δ*MTS-transfected cells, while the total Her2 expression was similar in wild-type, MTS, and *Δ*MTS cells (Fig. 9H). These results strongly indicate that the mitochondrial Her2 pool determines the sensitivity of MCF7 cells to MitoTam.

Discussion

Despite considerable advances in molecular oncology, cancer remains one of the leading causes of premature death (44). Breast cancer is the most frequent carcinoma in females, responsible for a high number of fatalities, and some subtypes are very hard to manage (6). Tamoxifen is commonly used as a first-line therapy of ER-positive breast cancer. However, almost 50% of patients develop resistance caused by multiple molecular reasons. One of these is the overexpression of the *HER2/neu* (also referred to as *ERBB2*) oncogene (45). Taking the high percentage of relapsed patients and possible side effects into consideration (5, 6), there is a demand for new generation of efficient drugs.

Based on the above, we designed and synthesized MitoTam, a tamoxifen derivative where the original tamoxifen moiety is conjugated to the mitochondria-targeting TPP$^+$ group (*cf* Fig. 1A). As predicted, this caused substantial accumulation of

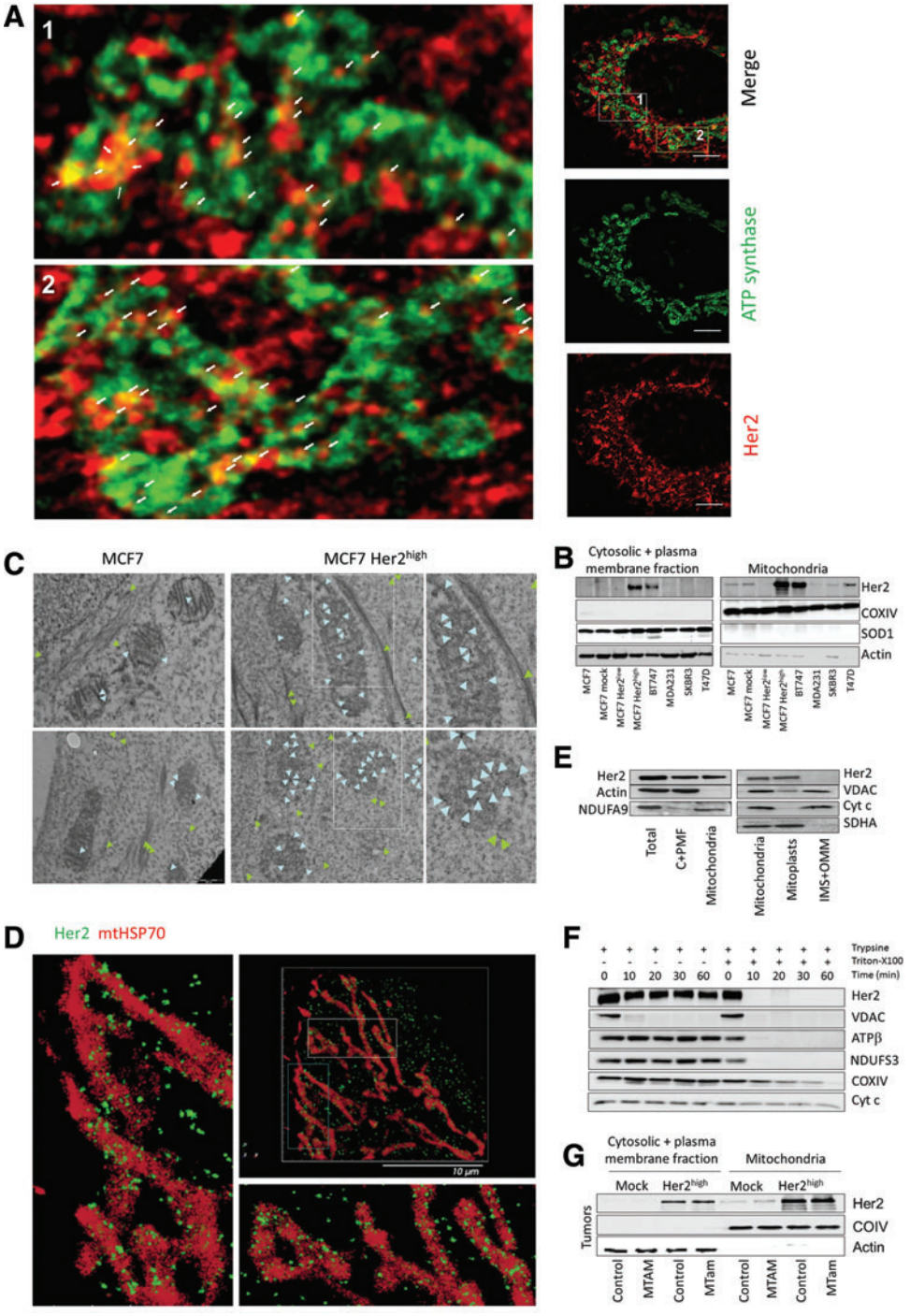

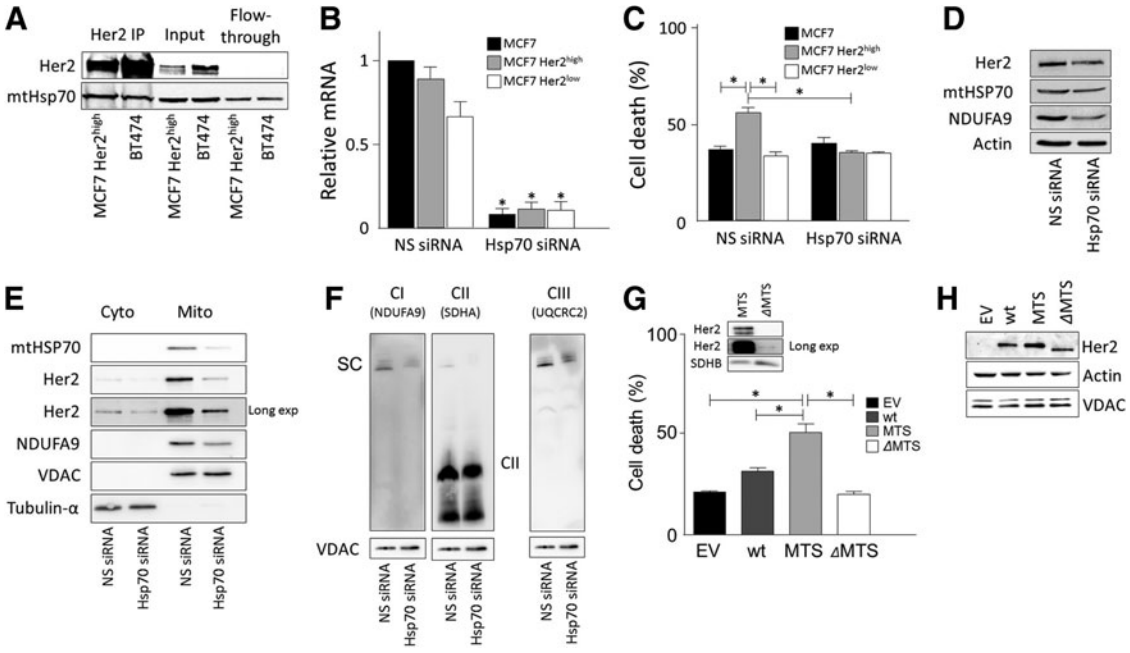

FIG. 9. Mitochondrial fraction of Her2 determines sensitivity to MitoTam. **(A)** Mitochondrial fractions of MCF7 Her2^{high} and BT474 cells were immunoprecipitated with anti-Her2 IgG and the immunoprecipitate, input, and flow-through inspected for Her2 and mtHsp70 by WB after SDS-PAGE. **(B)** MCF7 Her2^{high} cells transfected with mtHSP70 siRNA or NS siRNA were assessed for Her2 using qPCR. **(C)** MCF7, MCF7 Her2^{low}, and MCF7 Her2^{high} cells were transfected with siRNA against mtHSP70 or with NS siRNA, left to recover for 24 h, and then exposed to 2 μM MitoTam for 24 h and assessed for cell death. **(D)** MCF7 Her2^{high} cells were transfected with mtHSP70 siRNA or NS siRNA and the whole cell lysates were assessed for Her2, NDUFA9, and mtHSP70 by WB; Actin was used as a loading control. **(E)** MCF7 Her2^{high} cells were transfected with mtHSP70 siRNA or NS siRNA, and cytoplasmic and mitochondrial fractions were assessed for Her2 and NDUFA9 by WB. VDAC and tubulin-α were used as a loading controls. **(F)** MCF7 Her2high cells were transfected with mtHSP70 siRNA or NS siRNA, and the solubilized mitochondria were assessed for NDUFA9, SDHA (probed after NDUFA9 using the same membrane), and UQCRC2 by WB after NBGE. VDAC was used as a loading control. **(G)** MCF7 cells transiently transfected with empty vector, wild-type Her2, Her2-MTS, or Her2-ΔMTS were exposed to 2 μM MitoTam for 24 h and assessed for cell death. Insert shows the protein level of Her2 in mitochondrial fraction in MTS- and ΔMTS-transfected cells. SDHB was used as a loading control. **(H)** Whole cell lysates of transiently transfected cells show an even level of Her2. Actin and VDAC were used as loading controls. The symbol, *, indicates statistically significant difference between cells transfected with NS and mtHSP70 siRNA **(B)**, between MCF7, MCF7 Her2^{high}, and MCF7 Her2^{low} cells transfected with NS or mtHsp70 and MCF7 Her2^{high} cells transfected with NS and mtHsp70 cells **(C)**, and MCF7 cells transfected with wt, MTS, or ΔMTS plasmids **(G)**. Images **(A, D–H)** are representatives of at least three independent experiments. MTS, mitochondrial targeting sequence.

the modified compound at the matrix/IMM interface and led to a number of striking functional consequences. We found that MitoTam (i) kills a variety of breast cancer cells with a much higher efficacy than tamoxifen; (ii) in stark contrast to tamoxifen, is more efficient in killing Her2^{high} than Her2^{low} cells; (iii) very efficiently suppresses experimental Her2^{high} breast carcinomas; (iv) acts by suppression of CI-dependent respiration and disruption of respiratory SCs, which is particularly apparent in the Her2^{high} background; and (v) relies on the presence of mitochondrial fraction of Her2 protein for high efficacy in Her2^{high} cells/tumors.

TPP$^+$ tagging of tamoxifen makes it ideally suited for interaction with the ETC located at the matrix/IMM interface. We have shown recently that TPP$^+$ modification accentuates the propensity of medium affinity CII inhibitors to generate ROS (9, 17). In the current study, we detected substantial ROS generation upon MitoTam treatment, whereas very little or no ROS were induced by tamoxifen. ROS were functionally relevant as application of antioxidants protected from MitoTam-induced cell death. Given the previously published report that tamoxifen at supra-pharmacological concentrations inhibits CI (25), we considered the possibility that TPP$^+$-driven accumulation of the inhibitor in the vicinity of the ETC might result in accelerated CI inhibition. Indeed, MitoTam avidly and instantaneously suppressed CI-dependent respiration and CI-CIII oxidoreductase activity in cultured cells and in tumors (but not in the liver, demonstrating selectivity), while its effect on CII-driven respiration or CII-CIII oxidoreductase activity was low.

In addition, cell death induced by MitoTam was significantly reduced in a cellular model of CI deficiency, and molecular modeling suggested that MitoTam interacts within the UbQ binding cavity of CI. Importantly, such interaction would induce ROS in CI functioning in the forward manner expected to occur in intact cells (19, 52), explaining the experimental observations. Even though we cannot completely discount a contribution of downstream ETC components such as CIII and CIV to MitoTam-induced ROS formation and cell death, based on the available evidence, we propose that CI is the molecular target of MitoTam in mitochondria.

In contrast to tamoxifen, MitoTam proved very efficient in eliminating Her2^{high} breast cancer cells and tumors in multiple Her2^{high} models. In some instances, MitoTam application in mice led to complete regression of Her2^{high} tumors (*c.f.* Fig. 3), with no detectable relapse over the 8-month period after cessation of treatment. In addition, MitoTam suppressed invasiveness and metastasis formation, in line with reports that elevated oxidative stress reduces metastases (32, 59). Her2 overexpression sensitized both MCF7 and MDA-MB-231 cell lines to MitoTam even though these cell lines differ in their ER status. This indicates that Her2-associated sensitivity is independent of estrogen signaling. Interestingly, we discovered that Her2^{high} cells and tumors express more CI and that they have higher level of SCs, including the respirasome (1, 21, 24, 51), and that Her2^{high} cells and tumors feature higher oxygen consumption with CI substrates. In addition, we found that MitoTam treatment of Her2^{high} cells and mice bearing Her2^{high} tumors disrupted ETC SCs, which was much less apparent in cells with low Her2.

MitoTam also induced more mitochondrial ROS in Her2^{high} cells. Taken together, with more CI available, Her2^{high} cells may have higher capacity to generate ROS upon CI inhibition. This effect might be further amplified in a positive feedback loop by the MitoTam-mediated disruption of ETC SCs. This is consistent with the notion that SCs are viewed as conduits facilitating passage of reduced electron carriers such as UbQ within the ETC (21, 24) and prevent premature escape of electrons, limiting ROS formation. Hence, disruption of SCs, possibly by direct MitoTam binding or by initial ROS produced from CI, could amplify the overall rate of ROS generation specifically in Her2^{high} background and push the Her2^{high} cells over the threshold to cell death.

The results discussed above raise the possibility that Her2 overexpression could directly sensitize mitochondria to MitoTam. Several oncogenes have been reported in mitochondria (40), and one study recently suggested that a fraction of cellular Her2 also translocates into that organelle and stimulates glycolysis (7). We detect Her2 in mitochondria in our experimental breast cancer *in vitro* and *in vivo* models using several independent techniques and document that a significant portion of the cellular Her2 is localized at the cristae region of the IMM. In contrast to Ding *et al.* (7), we consistently find increased respiration in Her2^{high} cells and tumors, in line with increased SC assembly. Two pieces of evidence indicate that the mitochondrial fraction of Her2 is functionally relevant for the sensitization to MitoTam. First, the knockdown of mtHSP70, which mediates mitochondrial Her2 import (7), desensitized Her2^{high} cells to MitoTam, while no effect was observed in parental cells. Second, overexpression of Her2 constructs with increased and decreased ability to localize into mitochondria increased and decreased, respectively, sensitivity to MitoTam.

The reason why mitochondrial Her2 sensitizes to MitoTam is not entirely clear, but is very likely connected to IMM localization of Her2 in the proximity of ETC. The reduction of mitochondrial Her2 upon mtHSP70 knockdown reduced the SCs, including the respirasome, and Ding *et al.* reported Her2 interaction with complex IV of ETC (7). Because the assembly of the respirasome occurs only in the presence of CIII and CIV (21, 26, 51), Her2 could affect this process by facilitating respirasome assembly at the level of CIV, even though our data suggest that MitoTam interacts directly with CI.

In summary, we show that mitochondrial targeting of tamoxifen enhances its efficacy and broadens its applicability by imparting an additional biological activity directed at the ETC. This introduces MitoTam into the family of mitocans, anticancer agents acting directly on mitochondria, as first shown for the selective agent α-tocopheryl succinate (29, 30) targeting CII (8, 11). The role of CI in cancer is undoubtedly complex and context dependent (15, 41), but its pharmacological modulation might represent an effective approach to cancer therapy as demonstrated in this report. A novel finding that oncogenes such as Her2 might modulate the supramolecular organization of ETC and, in this way, determine the amount of ROS produced upon CI inhibition strengthens the paradigm of ETC targeting as a relevant approach for selective suppression of cancer (20, 38, 39, 54, 58).

Interestingly, various treatment-resistant and metastatic subpopulations of cancer cells show a high dependence on mitochondrial respiratory function, even though the information about ETC supramolecular organization into SCs in this context is limited (14, 22, 36, 51, 55). Accordingly, ETC-targeting agents such as MitoTam might provide means to eradicate these resistant populations, as documented in this report by efficient suppression of the hard-to-manage Her2^{high} breast carcinomas. MitoTam already passed the preclinical testing where it showed a very favorable toxicity profile and continues to phase I clinical trials.

Materials and Methods

Reagents

All reagents were from Sigma Aldrich (St. Louis, MO), unless stated otherwise.

Cell culture

Human breast cancer cell lines, MCF7 and MDA-MB-453, were obtained from the ATCC. BT474, MDA-MB-231, MDA-MB-436, SK-BR-3, and T47D human breast cancer cell lines were from J. A. López (Griffith University, Australia). The mouse NeuTL breast cancer cell line was originally derived from spontaneous breast carcinomas of FVB/N *c-neu* mice (13). The cells were cultured in DMEM (Lonza, Basel, Switzerland) with 10% FBS and 1% antibiotics in a 5% CO_2, 37°C, incubator. The 6-thioguanine-resistant mouse 4T1 cell line from ATCC was maintained in RPMI1640 (Lonza). Tamoxifen-resistant MCF7 cells were prepared by cultivation of MCF7 cells in the presence of escalating doses of tamoxifen for over 1 year. Chinese hamster lung fibroblasts B1 and B10 were from Prof. I. Scheffler (46). Human foreskin fibroblasts A014578, rat cardioblasts H9c2, and human immortalized endothelial EAhy926 cells were from the ATCC. All cell lines were authenticated. Mammospheres were generated and cultured as described (49).

Primary antibodies

The primary antibodies used were Her2 (OP-15; Calbiochem, San Diego, CA, or Ab-1221/1222; Sigma Aldrich), mtHsp70 (MA3-028; Thermo Scientific, Waltham, MA), Actin-HRP (5125; Cell Signaling, Danvers, MA), Caspase-9 (9501; Cell Signaling), Procaspase-9 (9508; Cell Signaling), Parp 1/2 (sc7150; Santa Cruz, Dallas, TX), Bax (2772; Cell Signaling), Bcl-2 (sc7382; Santa Cruz), Hsp60 (4870,

Cell Signaling), NDUFA9 (459100; Life Technologies, Carlsbad, CA), NDUFS3 (459103; Life Technologies), NDUFV1 (ab5535; Abcam; Cambridge, United Kingdom), SDHA(ab14715; Abcam), SDHA (ab14715; Abcam), SDHB (ab14714; Abcam), CoreI (459140; Life Technologies), Cox5a (453120; Life Technologies), CoxIV (4844; Cell Signaling), Atpβ (14730; Abcam; or kind gift from J. Houstek, Institute of Physiology CAS, used for imaging), mt-ND1 (74257; Abcam), Cyt c (sc13156; Santa Cruz), SOD1 (sc-11407; Santa Cruz), VDAC (4866; Cell Signaling), and β-tubulin-HRP (ab40742; Abcam).

DNA constructs and cell transfections

MCF7 cells with silenced expression of *Her2* oncogene were prepared by stable transfection with shRNA vectors (KH00209N; SA Biosciences, Frederick, MD). Full-length human Her2 construct was produced by PCR amplification of cDNA isolated from MDA-MB-453 cells using proofreading PFU DNA polymerase (Fermentas, Waltham, MA) and primers 5′-ATA AAG CTA GCC TCG AGC ACC ATG GAG CTG GCG G-3′ (forward) and 5′-ATA AAT CTA GAG AAT TCT CAC ACT GGC ACG TCC AGA C-3′ (reverse). The PCR product was gel-purified, digested with *Xho*I/*Xba*I (Takara, Mountain View, CA), repurified, and ligated between the *Xho*I and *Xba*I sites of pEF/IRES/Puro plasmid. MCF7 and MDA-MB-231 cells overexpressing Her2 were prepared by electroporation. Empty vectors were used as a control (mock transfection). Stable clones were selected by puromycin and verified by WB. Transient transfections with modified Her2-containing vectors were done using Lipofectamine 3000 (Thermo Scientific).

To obtain the Her2-MTS construct, Cox8-derived MTS was PCR-amplified from the pTagGFP2-mito vector (Evrogen, Moscow, Russia) using primers 5′-ATA AAG CTA GCC ACC ATG TCC GTC CTG ACG CCG CTG-3′ (forward) and 5′-ATA AAC TCG AGC TTG GAT CCC CCA ACG AAT G-3′ (reverse), gel-purified, digested by *Nhe*I/*Xho*I fast digestion enzymes (Thermo Scientific), repurified, and ligated between the *Nhe*I and *Xho*I sites in front of the full-length *Her2* cDNA in the pEF/IRES/Puro plasmid.

The Her2-ΔMTS construct was prepared by deletion of the internal mitochondria-targeting sequence reported by Ding *et al.* (7) from the full-length *Her2* cDNA in the pEF/IRES/Puro plasmid by inverse PCR using Q5 high-fidelity DNA polymerase in the presence of a GC enhancer (New England Biolabs, Ipswich, MA). The PCR product was agarose gel-purified and self-ligated by T4 ligase (Thermo Scientific). Primers for the inverse PCR reaction were phosphorylated by T4 oligonucleotide kinase (Thermo Scientific) before use, and their sequences were 5′-CTG CAG GAA ACG GAG CTG GTG GAG-3′and 5′-GCA TGC GCC CTC CTC ATC TGG-3′. All constructs were verified by DNA sequencing.

MCF7 cells with GFP-labeled mitochondria were prepared by stable transfection with pTagGFP2-mito vector using Fugene transfection reagent (Promega, Madison, WI). Transfections with siRNAs, where indicated in the figure legends, were performed using DharmaFect 1 reagent (Thermo Scientific). siRNAs for mtHsp70 (SASI_Hs01_00216924) and universal nonsilencing control siRNA were purchased from Sigma Aldrich.

Cell death and viability assays

Cell death was quantified by using the Annexin V-FITC/propidium iodide (PI) method and assessed by flow cytometry (FACSCalibur or FACSCanto; Becton Dickinson, Franklin Lakes, NJ). Proliferation was estimated using crystal violet staining. Cell death in the mammosphere model was assessed by PI (5 ng/ml, 5 min) staining and visualized by wide-field fluorescence microscopy (Nikon Ti-E, 10× lens).

Detection of ROS levels and mitochondrial inner membrane potential

The levels of ROS were evaluated using 2′,7′-dichlordihydrofluorescein diacetate (DCF) or MitoSOX (Life Technologies). Mitochondrial inner membrane potential was detected using tetramethylrhodamine methyl ester (TMRM). Cells were incubated with both probes under normal culture conditions for the times indicated, followed by evaluation using flow cytometry (50 n*M* TMRM, 5 μM DCF, 0.5 μM MitoSOX) or time-lapse confocal microscopy (10 n*M* TMRM).

Glucose uptake, lactate production, and ATP measurements

Glucose uptake was measured after 24 h of incubation in low-glucose DMEM and 15 min of preincubation with 50 μM 2-nitrobenzodeoxyglucose (2-NBDG; Life Technologies) by flow cytometry. For lactate production and ATP measurements, the cells were seeded in a 96-well format (10^4 per well) and the assays were performed as described (51).

Assessment of respiration of cells and tissue

Routine respiration and respiration *via* CI and CII were assessed using the high-resolution Oxygraph-2k respirometer (O2k; Oroboros Instruments, Innsbruck, Austria) according to the standard procedure (16, 31). For CI- and CII-dependent respiration, digitonin-permeabilized cells suspended in mitochondrial respiration medium, MiR05, were used in all experiments. The total oxygen concentration and consumption were monitored in the presence of specific inhibitors and substrates of CI (rotenone or glutamate/malate, respectively) or CII (malonate or succinate, respectively) in the presence of increasing concentrations of tamoxifen or MitoTam. Tissue respiration was assessed in an analogous manner using freshly excised tumor or liver homogenized in a dedicated tissue shredder. Respiration was monitored within 1 h after mice were sacrificed to avoid deterioration of the tissue.

Enzymatic assays

Isolated mitochondria were used after freeze–thaw treatment and hypotonic lysis. For NADH-cytochrome c oxidoreductase (CI-CIII) activity, 20 μg of mitochondria were incubated with 50 m*M* Tris (pH 8.0), 1 m*M* KCN, 2.5 mg/ml BSA, and 1 m*M* NADH at 30°C. Reaction (1 ml volume) was started by the addition of 40 μM cytochrome c, absorbance at 550 nm was followed for 90 s, and rotenone (5 μg/ml) was added for another 90 s. Rotenone insensitive rate was subtracted. Succinate-cytochrome c (CII-CIII) oxidoreductase activity was measured similarly, only NADH was replaced by 10 m*M* succinate and rotenone by 3 μM antimycin. Citrate

synthase was measured as described (48), but the reaction was scaled down into a 96-well plate format (200 μl volume).

Cellular and subcellular fractionation

Cells were washed twice with PBS, harvested by scrapping, and suspended in STE buffer (250 m*M* sucrose, 10 m*M* Tris, 1 m*M* EDTA) containing protease inhibitors. Suspension was homogenized on ice using a glass–Teflon homogenizer; mitochondrial fraction was isolated by differential centrifugation as detailed before (51). For preparation of mitoplasts, isolated mitochondria were recentrifuged at 10,000 *g*, the pellet resuspended in the hypotonic buffer (10 m*M* MOPS-KOH, pH 7.2, 1 m*M* EDTA), and incubated on ice for 30 min with occasional pipetting. The efficiency of the swelling reaction was confirmed by WB for selected IMM, IMS, and matrix proteins with parallel reaction of intact mitochondria incubated in the SEM buffer (10 m*M* MOPS-KOH, pH 7.2, 250 m*M* sucrose, 1 m*M* EDTA).

Protease protection assay

To determine mitochondrial residence of Her2, crude mitochondria were pelleted *via* centrifugation (10,000 *g*, 10 min, 4°C), resuspended to 0.5 mg/ml in the SEM buffer, and treated with 50 μg/ml trypsin in the presence or absence of 1% Triton X-100. The protease was inhibited by addition of 1 mg/ml soybean trypsin inhibitor at indicated times and the sample was processed for WB analysis.

Electrophoresis and Western blot analysis

SDS-PAGE, NBGE, and WB analysis were performed according to standard protocols as detailed elsewhere (51).

TUNEL assay

Excised tumors were mounted into paraffin blocks and sectioned. Tissue slices were deparaffinized and rehydrated. Apoptosis was detected using Click-iT TUNEL Alexa Fluor 488 assay (Invitrogen, Carlsbad, CA) according to the manufacturer's instructions.

Animal studies

Balb-c *nu/nu* mice were implanted with a slow-release estradiol pellet (60-day release of 12 μg per day; Innovative Research of America, Sarasota, FL) and injected subcutaneously (s.c.) with MCF7 mock or MCF7 Her2^{high} cells at 2×10^6 cells/animal. When tumors reached the volume of 30–50 mm^3 (quantified by ultrasound imaging, USI), mice were treated with either tamoxifen (2 μmol/mouse/dose), MitoTam (0.25 μmol/mouse/dose), or solvent control (4% ethanol in corn oil, 100 μl per dose) given intraperitoneally (i.p.) twice per week. FVB/N *c-neu* mice were s.c. injected with syngeneic NeuTl cells (13) at 2×10^6 cells/animal and treated as above with tamoxifen (2.69 μmol/mouse/dose) or MitoTam (0.54 μmol/mouse/dose). Tumor volume was monitored by the USI instrument Vevo770 (VisualSonics, Toronto, Canada).

For spontaneous Her2^{high} tumor treatment, FVB/N *c-neu* mice that developed tumors (450 mm^3 on average) were treated with MitoTam (0.54 μmol/mouse/dose) or solvent as above. For metastasis measurements, Balb/c mice were s.c. injected with 1×10^6 4T1 cells. After 1 week (when tumors reached on average 100 mm^3), MitoTam (0.25 μmol/mouse/dose) or solvent was administered as above for 2 weeks. The mice were sacrificed, blood, lungs, and liver were collected, single-cell suspension was prepared, and the metastatic cells were selected with 6-thioguanine for 10 days as described (34). The number of 6-thioguanine-resistant colonies was counted and expressed on per-organ basis. Animal weight was regularly monitored. Individual experimental groups contained at least five mice. All experiments were approved by the Czech academy of Sciences or Griffith University Ethics Committee and performed according to the Czech or the Australian and New Zealand Council guidelines for the Care and Use of Animals in Research and Teaching.

Zone exclusion assay

A total of 7×10^4 cells were seeded into glass-bottom microscopy plates using two-well silicone inserts (Ibidi, Martinsried, Germany). Three days after seeding, the inserts were removed, and MitoTam (0.5 μM) or solvent control was added. The plates were inspected by Nikon Ti-E wide-field microscope using a 10× lens at the time of insert removal and after 24 and 48 h.

Time-lapse confocal microscopy

Cells were seeded on glass-bottom microscopy dishes coated with poly-L-lysine. Images were recorded the third day after seeding using 63x oil immersion lens of the SP5 confocal microscope (Leica Microsystems, Wetzlar, Germany) equipped with a heated CO_2 incubator as described in detail before (53). Time-lapse images were recorded every 5 min with the first image taken 5 min before adding the drug. The maximal projection of 2 μm z-stack is shown.

STED microscopy

Cells were grown on coverslips coated with poly-L-lysine, fixed with 4% paraformaldehyde the third day after seeding, permeabilized with 0.05% Triton X-100, 0.05% Tween-20 in PBS, blocked with 5% FBS, and incubated with primary antibodies against ATPβ and Her2 (OP-15; Calbiochem) and secondary antibodies conjugated with Alexa Fluor 488 or Alexa Fluor 555 (Life Technologies). The coverslips were mounted in a glycerol medium containing N-propyl gallate, and single focal plane images were recorded with 100× oil immersion lens of SP8 confocal microscope equipped with STED module with 660 nm depletion laser (Leica Microsystems) and white laser.

Double channel Biplane FPALM/dSTORM

Cells were grown on glass coverslips coated with poly-L-lysine. Immunocytochemistry of Her2 and mtHSP70 proteins was performed using respective primary antibodies and secondary antibodies conjugated with Alexa Fluor 647 and Cy3b (Life Technologies). Samples were mounted in the dSTORM buffer (10% glucose, 50 m*M* cysteamine, 169 U of glucose oxidase, 1.4 U of catalase; all in 10 m*M* NaCl, 50 m*M* Tris-HCl, pH 8.0). Images were obtained using the Biplane FPALM instrument (Vutara, Salt Lake City, UT) equipped with 60× water immersion objective.

Immunogold transmission electron microscopy

Cells were grown on coverslips and fixed with 3% paraformaldehyde and 0.1% glutaraldehyde in Sorensen's buffer (SB; pH 7.2–7.4). After washing in the SB buffer, cells were dehydrated in ethanol series and embedded in LR white resin by a standard procedure. Ultrathin sections (70–90 nm) mounted on gilded copper grids, blocked with 10% NGS in PBS with 0.1% Tween 20, 1% BSA, pH 7.4, were incubated with primary antibody against Her2 diluted 1:50 (mouse monoclonal IgG, OP-15) and then with secondary antibody diluted 1:30 (goat anti-mouse conjugated with 12-nm colloidal gold particles; Jackson ImmunoResearch Laboratories, West Grove, PA). Observations and acquisition were done using the FEI Morgagni 268 transmission electron microscope operated at 80 kV (Fei Morgagni, Hillsboro, OR). The images were captured with the Mega View III CCD camera (Olympus, Tokyo, Japan). Multiple sections of at least three independent immunogold labeling experiments were analyzed.

Molecular modeling

The prereleased crystal structure of yeast complex I from Yarrowia lipolytica (PDB ID 4wz7) was kindly provided by the authors (60). The geometry of MitoTam was optimized using the DFT-D method (4). MitoTam was then allowed to sample docking poses in a box ($90 \times 90 \times 90$ grid points, 1.0 Å spacing) covering the lower part of the peripheral arm (Q module) and the transmembrane P_P module of the membrane arm. The Python Molecular Viewer (PMV 1.5) genetic algorithm steps each were collected employing AutoDock version 4.2 (27). The program 3V (56) was used to identify internal cavities connecting the iron–sulfur clusters with the UbQ binding site in the crystal structure.

Synthesis of tamoxifen derivatives

The synthesis of MitoTam and the derivatives used in this study (Supplementary Fig. S1) will be described in a separate publication (J.S. *et al.*, under preparation).

Statistical analysis

Data were analyzed in GraphPad Prism 5.04 software (GraphPad Software, La Jolla, CA) using unpaired Student's *t*-test analysis or two-way ANNOVA for comparisons of more than two parameters. Data shown are mean values ± SEM of at least three independent experiments (unless stated otherwise). A statistical difference of $p < 0.05$ was considered significant.

Acknowledgments

This research was supported in part by grants from the Australian Research Council (DP110105009) to J.N. and L.F.D., from the National and Health Medical Research Council of Australia (APP1011955), the Australian Research Council (DP130101651, DP15010280) the Cancer Council Queensland (APP1049104) to J.N., by the Czech Science Foundation grants to J.N. (16-12719S), J.R. (16-22823S) and J.T. (13-28830S and 16-12816S), by the Technology Agency of the Czech Republic (TE01020118), Ministry of Industry and Trade of the Czech Republic (FR-TI3/588), Institutional Research Support (RVO: 68378050) to M.S. and P.H., by the BIOCEV European Regional Development Fund CZ.1.05/1.100/02.0109 and the LQ1604 project of the National Sustainability Program II by the Ministry of Education, Youth and Sports.

Author Contributions

K. R., L. D., and J. N. designed the study; K. R., K. S., J. S., A. B., J. B., B. E., R. Z., J. G., T. S., E. A. P., B. Y., M. N. N., M. V., M. S., J. T., J. R., and L. D. performed experiments; J. S. and L. W. designed, synthetized, and analyzed compounds used in the study; J. C. performed molecular modeling; P. J. and P. H. supervised PALM and TEM studies; K. R., K. S., J. R., L. D., and J. N. analyzed and interpreted data; K. R., J. R., and J. N. wrote the manuscript; and J. N. supervised the study.

Author Disclosure Statement

J.N. and J.S. are inventors of a patent, 'Tamoxifen analogs for treatment of neoplastic diseases, especially with high Her2 protein level'. The authors declare no additional competing financial interests.

References

1. Acin-Perez R, Fernandez-Silva P, Peleato ML, Perez-Martos A, and Enriquez JA. Respiratory active mitochondrial supercomplexes. *Mol Cell* 32: 529–539, 2008.
2. Althoff T, Mills DJ, Popot JL, and Kuhlbrandt W. Arrangement of electron transport chain components in bovine mitochondrial supercomplex I1III2IV1. *EMBO J* 30: 4652–4664, 2011.
3. Birsoy K, Wang T, Chen WW, Freinkman E, Abu-Remaileh M, and Sabatini DM. An essential role of the mitochondrial electron transport chain in cell proliferation is to enable aspartate synthesis. *Cell* 162: 540–551, 2015.
4. Cerny J, Jurecka P, Hobza P, and Valdes H. Resolution of identity density functional theory augmented with an empirical dispersion term (RI-DFT-D): a promising tool for studying isolated small peptides. *J Phys Chem A* 111: 1146–1154, 2007.
5. Dawood S, Broglio K, Buzdar AU, Hortobagyi GN, and Giordano SH. Prognosis of women with metastatic breast cancer by HER2 status and trastuzumab treatment: an institutional-based review. *J Clin Oncol* 28: 92–98, 2010.
6. DeSantis CE, Lin CC, Mariotto AB, Siegel RL, Stein KD, Kramer JL, Alteri R, Robbins AS, and Jemal A. Cancer treatment and survivorship statistics, 2014. *CA Cancer J Clin* 64: 252–271, 2014.
7. Ding Y, Liu Z, Desai S, Zhao Y, Liu H, Pannell LK, Yi H, Wright ER, Owen LB, Dean-Colomb W, Fodstad O, Lu J, LeDoux SP, Wilson GL, and Tan M. Receptor tyrosine kinase ErbB2 translocates into mitochondria and regulates cellular metabolism. *Nat Commun* 3: 1271, 2012.
8. Dong LF, Freeman R, Liu J, Zobalova R, Marin-Hernandez A, Stantic M, Rohlena J, Valis K, Rodriguez-Enriquez S, Butcher B, Goodwin J, Brunk UT, Witting PK, Moreno-Sanchez R, Scheffler IE, Ralph SJ, and Neuzil J. Suppression of tumor growth in vivo by the mitocan alpha-tocopheryl succinate requires respiratory complex II. *Clin Cancer Res* 15: 1593–1600, 2009.
9. Dong LF, Jameson VJ, Tilly D, Cerny J, Mahdavian E, Marin-Hernandez A, Hernandez-Esquivel L, Rodriguez-Enriquez S, Stursa J, Witting PK, Stantic B, Rohlena J,

Truksa J, Kluckova K, Dyason JC, Ledvina M, Salvatore BA, Moreno-Sanchez R, Coster MJ, Ralph SJ, Smith RA, and Neuzil J. Mitochondrial targeting of vitamin E succinate enhances its pro-apoptotic and anti-cancer activity via mitochondrial complex II. *J Biol Chem* 286: 3717–3728, 2011.

10. Dong LF, Jameson VJ, Tilly D, Prochazka L, Rohlena J, Valis K, Truksa J, Zobalova R, Mahdavian E, Kluckova K, Stantic M, Stursa J, Freeman R, Witting PK, Norberg E, Goodwin J, Salvatore BA, Novotna J, Turanek J, Ledvina M, Hozak P, Zhivotovsky B, Coster MJ, Ralph SJ, Smith RA, and Neuzil J. Mitochondrial targeting of alpha-tocopheryl succinate enhances its pro-apoptotic efficacy: a new paradigm for effective cancer therapy. *Free Radic Biol Med* 50: 1546–1555, 2011.
11. Dong LF, Low P, Dyason JC, Wang XF, Prochazka L, Witting PK, Freeman R, Swettenham E, Valis K, Liu J, Zobalova R, Turanek J, Spitz DR, Domann FE, Scheffler IE, Ralph SJ, and Neuzil J. Alpha-tocopheryl succinate induces apoptosis by targeting ubiquinone-binding sites in mitochondrial respiratory complex II. *Oncogene* 27: 4324–4335, 2008.
12. Dontu G, Abdallah WM, Foley JM, Jackson KW, Clarke MF, Kawamura MJ, and Wicha MS. In vitro propagation and transcriptional profiling of human mammary stem/progenitor cells. *Genes Dev* 17: 1253–1270, 2003.
13. Guy CT, Webster MA, Schaller M, Parsons TJ, Cardiff RD, and Muller WJ. Expression of the neu protooncogene in the mammary epithelium of transgenic mice induces metastatic disease. *Proc Natl Acad Sci U S A* 89: 10578–10582, 1992.
14. Haq R, Shoag J, Andreu-Perez P, Yokoyama S, Edelman H, Rowe GC, Frederick DT, Hurley AD, Nellore A, Kung AL, Wargo JA, Song JS, Fisher DE, Arany Z, and Widlund HR. Oncogenic BRAF regulates oxidative metabolism via PGC1alpha and MITF. *Cancer Cell* 23: 302–315, 2013.
15. Kim EM, Park JK, Hwang SG, Kim WJ, Liu ZG, Kang SW, and Um HD. Nuclear and cytoplasmic p53 suppress cell invasion by inhibiting respiratory Complex-I activity via Bcl-2 family proteins. *Oncotarget* 5: 8452–8465, 2014.
16. Kluckova K, Dong LF, Bajzikova M, Rohlena J, and Neuzil J. Evaluation of respiration of mitochondria in cancer cells exposed to mitochondria-targeted agents. *Methods Mol Biol* 1265: 181–194, 2015.
17. Kluckova K, Sticha M, Cerny J, Mracek T, Dong L, Drahota Z, Gottlieb E, Neuzil J, and Rohlena J. Ubiquinone-binding site mutagenesis reveals the role of mitochondrial complex II in cell death initiation. *Cell Death Dis* 6: e1749, 2015.
18. Kordes S, Pollak MN, Zwinderman AH, Mathot RA, Weterman MJ, Beeker A, Punt CJ, Richel DJ, and Wilmink JW. Metformin in patients with advanced pancreatic cancer: a double-blind, randomised, placebo-controlled phase 2 trial. *Lancet Oncol* 16: 839–847, 2015.
19. Kussmaul L and Hirst J. The mechanism of superoxide production by NADH:ubiquinone oxidoreductase (complex I) from bovine heart mitochondria. *Proc Natl Acad Sci U S A* 103: 7607–7612, 2006.
20. Kwong JQ, Henning MS, Starkov AA, and Manfredi G. The mitochondrial respiratory chain is a modulator of apoptosis. *J Cell Biol* 179: 1163–1177, 2007.
21. Lapuente-Brun E, Moreno-Loshuertos R, Acin-Perez R, Latorre-Pellicer A, Colas C, Balsa E, Perales-Clemente E, Quiros PM, Calvo E, Rodriguez-Hernandez MA, Navas P, Cruz R, Carracedo A, Lopez-Otin C, Perez-Martos A, Fernandez-Silva P, Fernandez-Vizarra E, and Enriquez JA. Supercomplex assembly determines electron flux in the mitochondrial electron transport chain. *Science* 340: 1567–1570, 2013.
22. LeBleu VS, O'Connell JT, Gonzalez Herrera KN, Wikman H, Pantel K, Haigis MC, de Carvalho FM, Damascena A, Domingos Chinen LT, Rocha RM, Asara JM, and Kalluri R. PGC-1alpha mediates mitochondrial biogenesis and oxidative phosphorylation in cancer cells to promote metastasis. *Nat Cell Biol* 16: 992–1003, 1–15, 2014.
23. Lega IC, Austin PC, Gruneir A, Goodwin PJ, Rochon PA, and Lipscombe LL. Association between metformin therapy and mortality after breast cancer: a population-based study. *Diabetes Care* 36: 3018–3026, 2013.
24. Maranzana E, Barbero G, Falasca AI, Lenaz G, and Genova ML. Mitochondrial respiratory supercomplex association limits production of reactive oxygen species from complex I. *Antioxid Redox Signal* 19: 1469–1480, 2013.
25. Moreira PI, Custodio J, Moreno A, Oliveira CR, and Santos MS. Tamoxifen and estradiol interact with the flavin mononucleotide site of complex I leading to mitochondrial failure. *J Biol Chem* 281: 10143–10152, 2006.
26. Moreno-Lastres D, Fontanesi F, Garcia-Consuegra I, Martin MA, Arenas J, Barrientos A, and Ugalde C. Mitochondrial complex I plays an essential role in human respirasome assembly. *Cell Metab* 15: 324–335, 2012.
27. Morris GM, Huey R, Lindstrom W, Sanner MF, Belew RK, Goodsell DS, and Olson AJ. AutoDock4 and AutoDockTools4: automated docking with selective receptor flexibility. *J Comput Chem* 30: 2785–2791, 2009.
28. Murphy MP and Smith RA. Targeting antioxidants to mitochondria by conjugation to lipophilic cations. *Annu Rev Pharmacol Toxicol* 47: 629–656, 2007.
29. Neuzil J, Weber T, Gellert N, and Weber C. Selective cancer cell killing by alpha-tocopheryl succinate. *Br J Cancer* 84: 87–89, 2001.
30. Neuzil J, Weber T, Schroder A, Lu M, Ostermann G, Gellert N, Mayne GC, Olejnicka B, Negre-Salvayre A, Sticha M, Coffey RJ, and Weber C. Induction of cancer cell apoptosis by alpha-tocopheryl succinate: molecular pathways and structural requirements. *FASEB J* 15: 403–415, 2001.
31. Pesta D and Gnaiger E. High-resolution respirometry: OXPHOS protocols for human cells and permeabilized fibers from small biopsies of human muscle. *Methods Mol Biol* 810: 25–58, 2012.
32. Piskounova E, Agathocleous M, Murphy MM, Hu Z, Huddlestun SE, Zhao Z, Leitch AM, Johnson TM, DeBerardinis RJ, and Morrison SJ. Oxidative stress inhibits distant metastasis by human melanoma cells. *Nature* 527: 186–191, 2015.
33. Prochazka L, Koudelka S, Dong LF, Stursa J, Goodwin J, Neca J, Slavik J, Ciganek M, Masek J, Kluckova K, Nguyen M, Turanek J, and Neuzil J. Mitochondrial targeting overcomes ABCA1-dependent resistance of lung carcinoma to alpha-tocopheryl succinate. *Apoptosis* 18: 286–299, 2013.
34. Pulaski BA and Ostrand-Rosenberg S. Mouse 4T1 breast tumor model. *Curr Protoc Immunol* Chapter 20: Unit 20 2, 2001.
35. Reni M, Dugnani E, Cereda S, Belli C, Balzano G, Nicoletti R, Liberati D, Pasquale V, Scavini M, Maggiora P,

Sordi V, Lampasona V, Ceraulo D, Di Terlizzi G, Doglioni C, Falconi M, and Piemonti L. (Ir)relevance of metformin treatment in patients with metastatic pancreatic cancer: an open-label, randomized phase 2 trial. *Clin Cancer Res* 22: 1076–1085, 2016.

36. Roesch A, Vultur A, Bogeski I, Wang H, Zimmermann KM, Speicher D, Korbel C, Laschke MW, Gimotty PA, Philipp SE, Krause E, Patzold S, Villanueva J, Krepler C, Fukunaga-Kalabis M, Hoth M, Bastian BC, Vogt T, and Herlyn M. Overcoming intrinsic multidrug resistance in melanoma by blocking the mitochondrial respiratory chain of slow-cycling JARID1B(high) cells. *Cancer Cell* 23: 811–825, 2013.
37. Rohlena J, Dong LF, Kluckova K, Zobalova R, Goodwin J, Tilly D, Stursa J, Pecinova A, Philimonenko A, Hozak P, Banerjee J, Ledvina M, Sen CK, Houstek J, Coster MJ, and Neuzil J. Mitochondrially targeted alpha-tocopheryl succinate is antiangiogenic: potential benefit against tumor angiogenesis but caution against wound healing. *Antioxid Redox Signal* 15: 2923–2935, 2011.
38. Rohlena J, Dong LF, and Neuzil J. Targeting the mitochondrial electron transport chain complexes for the induction of apoptosis and cancer treatment. *Curr Pharm Biotechnol* 14: 377–389, 2013.
39. Rohlena J, Dong LF, Ralph SJ, and Neuzil J. Anticancer drugs targeting the mitochondrial electron transport chain. *Antioxid Redox Signal* 15: 2951–2974, 2011.
40. Rohlenova K, Neuzil J, and Rohlena J. The role of Her2 and other oncogenes of the PI3K/AKT pathway in mitochondria. *Biol Chem* 397: 607–615, 2016.
41. Santidrian AF, Matsuno-Yagi A, Ritland M, Seo BB, LeBoeuf SE, Gay LJ, Yagi T, and Felding-Habermann B. Mitochondrial complex I activity and NAD+/NADH balance regulate breast cancer progression. *J Clin Invest* 123: 1068–1081, 2013.
42. Saura C, Bendell J, Jerusalem G, Su S, Ru Q, De Buck S, Mills D, Ruquet S, Bosch A, Urruticoechea A, Beck JT, Di Tomaso E, Sternberg DW, Massacesi C, Hirawat S, Dirix L, and Baselga J. Phase Ib study of Buparlisib plus Trastuzumab in patients with HER2-positive advanced or metastatic breast cancer that has progressed on Trastuzumab-based therapy. *Clin Cancer Res* 20: 1935–1945, 2014.
43. Schafer ZT, Grassian AR, Song L, Jiang Z, Gerhart-Hines Z, Irie HY, Gao S, Puigserver P, and Brugge JS. Antioxidant and oncogene rescue of metabolic defects caused by loss of matrix attachment. *Nature* 461: 109–113, 2009.
44. Siegel RL, Miller KD, and Jemal A. Cancer statistics, 2015. *CA Cancer J Clin* 65: 5–29, 2015.
45. Slamon DJ, Clark GM, Wong SG, Levin WJ, Ullrich A, and McGuire WL. Human breast cancer: correlation of relapse and survival with amplification of the HER-2/neu oncogene. *Science* 235: 177–182, 1987.
46. Soderberg K, Mascarello JT, Breen GA, and Scheffler IE. Respiration-deficient Chinese hamster cell mutants: genetic characterization. *Somatic Cell Genet* 5: 225–240, 1979.
47. Soderberg KL, Ditta GS, and Scheffler IE. Mammalian cells with defective mitochondrial functions: a Chinese hamster mutant cell line lacking succinate dehydrogenase activity. *Cell* 10: 697–702, 1977.
48. Spinazzi M, Casarin A, Pertegato V, Salviati L, and Angelini C. Assessment of mitochondrial respiratory chain enzymatic activities on tissues and cultured cells. *Nat Protoc* 7: 1235–1246, 2012.
49. Stapelberg M, Zobalova R, Nguyen MN, Walker T, Stantic M, Goodwin J, Pasdar EA, Thai T, Prokopova K, Yan B, Hall S, de Pennington N, Thomas SR, Grant G, Stursa J, Bajzikova M, Meedeniya AC, Truksa J, Ralph SJ, Ansorge O, Dong LF, and Neuzil J. Indoleamine-2,3-dioxygenase elevated in tumor-initiating cells is suppressed by mitocans. *Free Radic Biol Med* 67: 41–50, 2014.
50. Sullivan LB, Gui DY, Hosios AM, Bush LN, Freinkman E, and Vander Heiden MG. Supporting aspartate biosynthesis is an essential function of respiration in proliferating cells. *Cell* 162: 552–563, 2015.
51. Tan AS, Baty JW, Dong LF, Bezawork-Geleta A, Endaya B, Goodwin J, Bajzikova M, Kovarova J, Peterka M, Yan B, Pesdar EA, Sobol M, Filimonenko A, Stuart S, Vondrusova M, Kluckova K, Sachaphibulkij K, Rohlena J, Hozak P, Truksa J, Eccles D, Haupt LM, Griffiths LR, Neuzil J, and Berridge MV. Mitochondrial genome acquisition restores respiratory function and tumorigenic potential of cancer cells without mitochondrial DNA. *Cell Metab* 21: 81–94, 2015.
52. Treberg JR, Quinlan CL, and Brand MD. Evidence for two sites of superoxide production by mitochondrial NADH-ubiquinone oxidoreductase (complex I). *J Biol Chem* 286: 27103–27110, 2011.
53. Truksa J, Dong LF, Rohlena J, Stursa J, Vondrusova M, Goodwin J, Nguyen M, Kluckova K, Rychtarcikova Z, Lettlova S, Spacilova J, Stapelberg M, Zoratti M, and Neuzil J. Mitochondrially targeted vitamin E succinate modulates expression of mitochondrial DNA transcripts and mitochondrial biogenesis. *Antioxid Redox Signal* 22: 883–900, 2015.
54. Viale A, Corti D, and Draetta GF. Tumors and mitochondrial respiration: a neglected connection. *Cancer Res* 75: 3687–3691, 2015.
55. Viale A, Pettazzoni P, Lyssiotis CA, Ying H, Sanchez N, Marchesini M, Carugo A, Green T, Seth S, Giuliani V, Kost-Alimova M, Muller F, Colla S, Nezi L, Genovese G, Deem AK, Kapoor A, Yao W, Brunetto E, Kang Y, Yuan M, Asara JM, Wang YA, Heffernan TP, Kimmelman AC, Wang H, Fleming JB, Cantley LC, DePinho RA, and Draetta GF. Oncogene ablation-resistant pancreatic cancer cells depend on mitochondrial function. *Nature* 514: 628–632, 2014.
56. Voss NR and Gerstein M. 3V: cavity, channel and cleft volume calculator and extractor. *Nucleic Acids Res* 38: W555–W562, 2010.
57. Weinberg F, Hamanaka R, Wheaton WW, Weinberg S, Joseph J, Lopez M, Kalyanaraman B, Mutlu GM, Budinger GR, and Chandel NS. Mitochondrial metabolism and ROS generation are essential for Kras-mediated tumorigenicity. *Proc Natl Acad Sci U S A* 107: 8788–8793, 2010.
58. Wolf DA. Is reliance on mitochondrial respiration a ''chink in the armor'' of therapy-resistant cancer? *Cancer Cell* 26: 788–795, 2014.
59. Zhang Q, Raje V, Yakovlev VA, Yacoub A, Szczepanek K, Meier J, Derecka M, Chen Q, Hu Y, Sisler J, Hamed H, Lesnefsky EJ, Valerie K, Dent P, and Larner AC. Mitochondrial localized Stat3 promotes breast cancer growth via phosphorylation of serine 727. *J Biol Chem* 288: 31280–31288, 2013.
60. Zickermann V, Wirth C, Nasiri H, Siegmund K, Schwalbe H, Hunte C, and Brandt U. Structural biology. Mechanistic insight from the crystal structure of mitochondrial complex I. *Science* 347: 44–49, 2015.

Address correspondence to:
Dr. Jiri Neuzil
Mitochondria, Apoptosis and Cancer Research Group
School of Medical Science and Menzies Health Institute Queensland
Griffith University
Southport
Qld 4222
Australia

E-mail: j.neuzil@griffith.edu.au

Dr. Lan-Feng Dong
Mitochondria, Apotosis and Cancer Research Group
School of Medical Science and Menzies Health Institute Queensland
Griffith University
Southport
Qld 4222
Australia

E-mail: l.dong@griffith.edu.au

Katerina Rohlenova
Molecular Therapy Group
Institute of Biotechnology
Czech Academy of Sciences
25250 Prague-West
Czech Republic

E-mail: Katerina.rohlenova@ibt.cas.cz

Dr. Jakub Rohlena
Molecular Therapy Group
Institute of Biotechnology
Czech Academy of Sciences
25250 Prague-West
Czech Republic

E-mail: jakub.rohlena@ibt.cas.cz

Date of first submission to ARS Central, February 26, 2016; date of final revised submission, June 21, 2016; date of acceptance, June 27, 2016.

Abbreviations Used

$\Delta\Psi_{m,I}$ = mitochondrial inner membrane potential
CI, CII, CIII, CIV, CV = respiratory complex I, II, III, IV, V
ER = estrogen receptor
ETC = electron transport chain
FCCP = carbonyl cyanide 4-(trifluoromethoxy) phenylhydrazone
IMM = inner mitochondrial membrane
IMS = intermembrane space
MitoTam = mitochondrially targeted tamoxifen
MTS = mitochondrial targeting sequence
NAC = N-acetyl cysteine
NBGE = native blue gel electrophoresis
OMM = outer mitochondrial membrane
PI = propidium iodide
RC = respiratory complex
ROS = reactive oxygen species
SC = supercomplex
Tam-DPPO = Diphenylphosphine oxide tamoxifen
TMRM = tetramethylrhodamine methyl ester
TPP^+ = triphenylphosphonium
UbQ = ubiquinone
WB = Western blotting